Role of Spin Density Waves in Mechanism of Superconductivity in $Cu_{0.5}Tl_{0.5}Ba_2Ca_2Cu_{3-x}Zn_xO_{10-\delta}$ (x=0, 1, 2, 3) Sample

Maria Mushtaq

Department of Physics

Quaid-i-Azam University

Islamabad, Pakistan

2023

A dissertation submitted to the department of physics, Quaid-i-Azam University, Islamabad, in the partial fulfilment of the requirement for the degree of

Master of Philosophy in Physics

By

Maria Mushtaq

Materials Science Laboratory

Department of Physics

Quaid-i-Azam University

Islamabad, Pakistan

2023

CERTIFICATE

This is to certify that this thesis entitled as **'Role of Spin Density Waves in Mechanism of Superconductivity in $Cu_{0.5}Tl_{0.5}Ba_2Ca_2Cu_{3-x}Zn_xO_{10-\delta}$ (x=0, 1, 2, 3) Sample'** submitted by **Maria Mushtaq** is accepted in its present form by the department of Physics, Faculty of Natural Sciences, **Quaid-i-Azam University, Islamabad, Pakistan** as satisfying the thesis requirement for the degree of **Master of Philosophy (MPhil)** in **Physics.**

Supervisor

Prof. Dr. Nawazish Ali Khan

Department of Physics

Quaid-i-Azam University Islamabad, Pakistan

Chairman

Prof. Dr Kashif Sabeeh

Department of Physics

Quaid-i-Azam University Islamabad, Pakistan

Dated: _____

To Ammi and Abu,

Everything I do,

I do for you.

Acknowledgment

All praises to Allah's guidance and blessings throughout this research journey, for it is by His grace that I have been able to undertake and complete this academic endeavor**.** I would like to express my deepest gratitude to my supervisor, **Dr. Nawazish Ali Khan**, for his unwavering guidance, support, and mentorship throughout this research journey.

I would like to thank **Dr. Hamza Safeer** for his invaluable assistance with equipment, experiments, and data analysis.

I am also profoundly grateful to my family, especially my parents for their unwavering love and encouragement that have made my education and this thesis possible. Your faith in me has been my greatest motivation.

I owe a special debt of gratitude to my friend, **Aqsa Bashir**, for her unwavering emotional support and for being a constant source of encouragement.

This thesis was a journey filled with challenges, and I acknowledge the setbacks and difficulties that ultimately contributed to my personal and academic growth. As I conclude this thesis, I eagerly anticipate the future research and academic pursuits lying ahead, driven by the knowledge and experiences gained during this project.

Maria Mushtaq

Contents

List of Figures

List of Tables

Chapter 1

INTRODUCTION TO SUPERCONDUCTIVITY

In this chapter, we will utilise the fundamental characteristics of superconductors, basic experimental findings, and the theoretical frameworks to analyse the development of superconductivity. It includes the high temperature superconductors (HTSC), cuprates based on thallium, and their significant family of HTSC.

1.1 SUPERCONDUCTIVITY

In 1911, K. Onnes found that when the temperature of mercury is decreased and it reaches 4K, suddenly its resistivity vanishes **[1]**. This was a moment of triumph in the history of electrical resistance, and it opened a new area in the field of physics. This phenomenon was defined as superconductivity. In simple words, when the temperature of any material is decreased and upon reaching certain temperature, it loses all its resistivity then we define it as superconductivity. The temperature at which this phenomenon happens is termed as critical temperature.

Superconductivity is quantum mechanical phenomenon and there are two characteristics associated with superconducting state.

- Perfect diamagnetism
- Zero electrical resistance

Perfect diamagnetism shown by superconductors is also called Meissner effect, in which when a material transitions into superconducting state, the magnetic field is completely expelled from it **[2]**.

The electrical resistivity arises due to lattice vibrations and due to interaction of electrons with atoms. This resistivity vanishes in superconducting state because at lower temperature lattice vibrations stop. Also, there is no more interaction of electrons with impurities.

The superconducting state is also called more ordered state and this order is due to the loose pair of electrons. These electrons form cooper pairs below T_c and above T_c, they tend to lose their pairing. This ordering of electrons was explained by Bardeen, Cooper and

Schrieffer **[3]**. According to them, in superconducting state there is not only columbic repulsion between electrons but also there is an attractive force between them which give rise to the pairing effect.

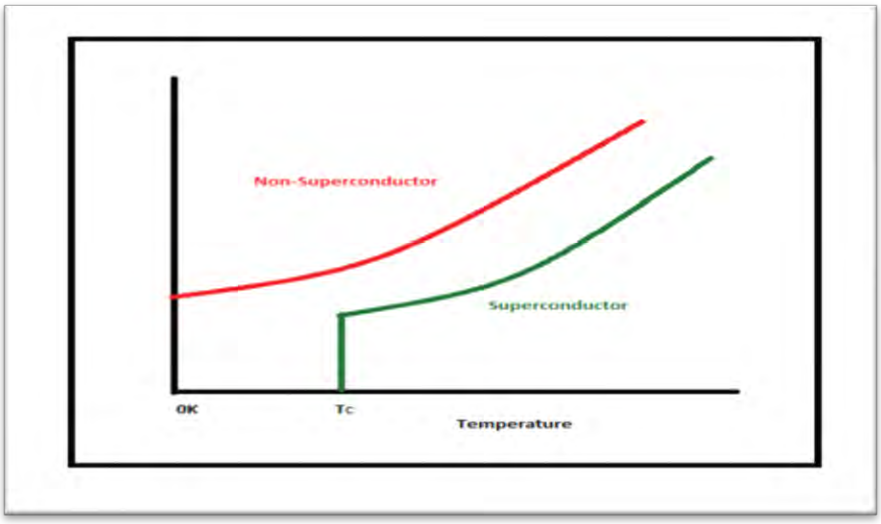

Figure 1.1 Resistance vs temperature curve for superconductors

1.2 HISTORY OF SUPERCONDUCTIVITY

H. Kamerlingh Onnes discovered superconductivity in 1911 just 3 years after he had first liquified helium **[4]**. Scientists working in the field struggled for decades to understand the phenomenon of superconductivity. Then in the 1950s and 1960s, a justifiable theoretical picture of superconductivity was emerged. For more than 75 years of its discovery, Superconductivity was popular to be a very low temperature phenomenon.

In 1984, L., S. Brizhik and, A. S. Davydov proposed a model to explain the phenomenon of superconductivity in quasi1-D conductors **[5]**. Due to the coupling of non-linear and strong electron-phonon interactions cooper pairs are quasi-one-dimensional excitations. They were awarded a Noble prize for this discovery in 1987. Scientists were astonished by this discovery because cuprates were considered as bad conductors. This was the cause of major attraction towards superconductivity because many of the scientists then realized that the superconducting phenomenon is different from normal conducting phenomenon.

P. Anderson proposed a model to explain the superconductivity in cuprates occurrence in 1987. He made the assumption that the pair mechanism and the formation of phase coherence are two distinct mechanisms in this paradigm **[6]**.

Scientific research was accelerated after the discovery of superconductivity in quasi1-D conductors. In 1988, superconducting properties were found in $Bi_2Sr_2Ca_{n-1}Cu_n0_{2n+2}$ and many other families of compounds **[7]**. Scientists struggled to achieve higher T_c and many succeeded to discover compound having transition temperature above *100K* at normal pressure. Later in 1989 Tl-based cuprates doped with rare earth oxides were found to be good superconductors. At normal pressure, $HgBa_2Ca_2Cu_3O_8$ is claimed to have maximum 'T_c' of *135K*.

Scientists carried on their research and found that by increasing external pressure, the superconductivity can be enhanced. Considering this observation, under an external pressure of *30GPa*, the transition temperature is increased to *164K* **[8]**. H_2S was found to have a critical temperature of *200K* at a pressure of *155GPa* **[9]**. Researchers continued their struggle to obtain higher T_c from the discovery of superconductivity till now. This struggle can be picturized as shown in Fig 1.2. Let's hope that one day we'll be using superconductors at ambient conditions.

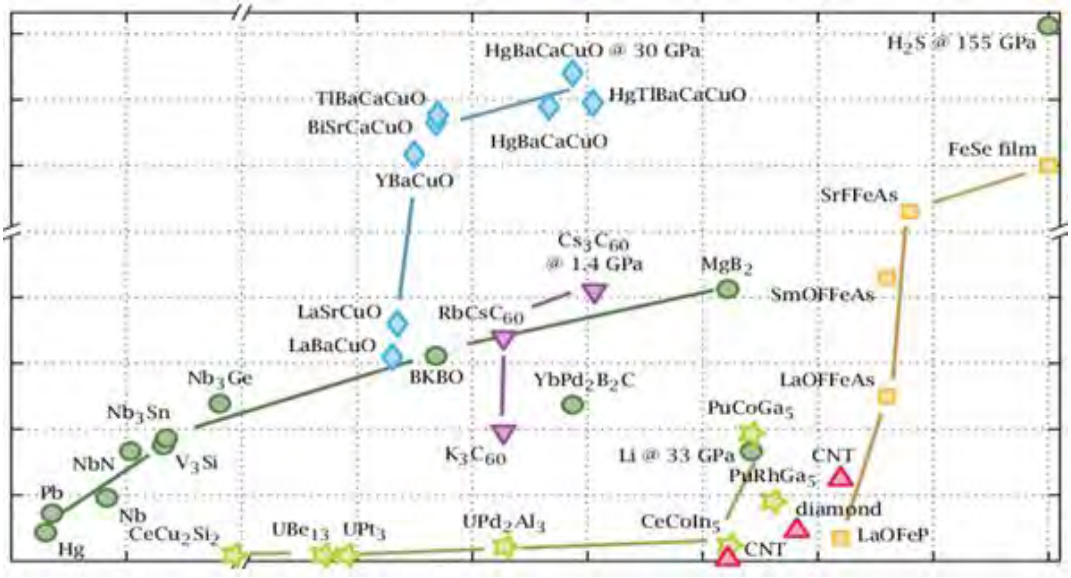

Figure 1.2 Discovery of superconductivity throughout the years (1900-2015)

1.3 TYPES OF SUPERCONDUCTORS

V.L. Ginzburg and L. Landau presented that there are two different kinds of superconductors **[10]**. They are divided into two classes on the basis of magnetic characteristics of superconductors.

1. Type I Superconductors

2. Type II Superconductors

1.3.1 Type I Superconductors

These superconductors obey Meissner effect i.e. exhibits ideal diamagnetism. BCS theory explains the isotropic nature of these materials. When the magnetic field, greater than their critical value H_c, is applied they quickly change their superconducting state to normal. Their diamagnetic state changes to paramagnetic state when the field greater than Hc is applied. Free energy of Type I superconductors is positive at the normal-superconducting interface. Only when applied magnetic field is less than the critical value, the surface current flows in these superconductors. For Type I superconductors Ginzburg-Landau parameter is always less than 1. They are also named as conventional superconductors. Only a very small value of critical magnetic field e.g, 0.2 tesla can completely destroy their superconductivity. Mercury, Lead, Strontium and their alloys are type I superconductors **[11]**.

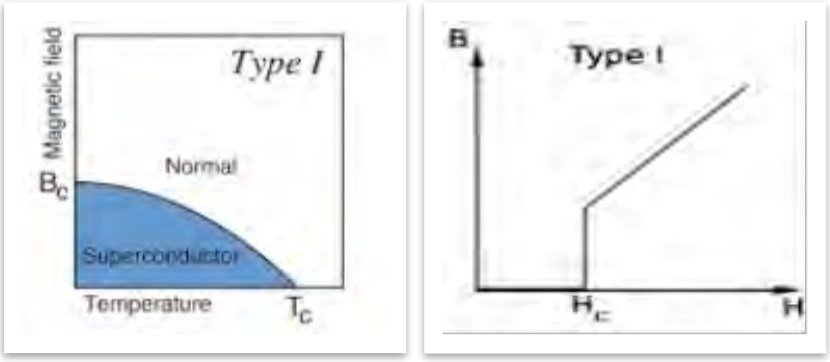

Fig 1.3: (a) H-T Phase diagram of Type I superconductors

(b) Resistivity vs. Temperature curve of Type I superconductors

1.3.2 Type-II Superconductors

L. Shubnikov made the initial discovery of type-II superconductors, and Alexei A.

Abrikosov further extended their idea. They do not follow the Meissner principle. The metallic state gradually replaces the superconducting state in these superconductors. It is impossible for magnetic flux to pass through the mass of a superconductor when the applied magnetic field H is less than the lower critical value H_{c1}. The material exhibits excellent diamagnetic nature in area $H < H_{c1}$.

Between H_{c1} and H_{c2} (upper critical field), superconductivity was only minimally hampered. Mixed or intermediate area is the phrase used to describe the region $H_{c1} < H < H_{c2}$. Magnetic flux penetrates into the mixed zone in the form of vortices. In the material, vortices are evenly distributed. Magnetic field lines can enter the material in the region $H > H_{c2}$, which destroys superconductivity. The GL parameter for type-II superconductors is bigger than unity **[12]**. They are also named as unconventional superconductors. They have a higher critical temperature than type-I superconductors. These types of superconductors include silicon, boron-doped diamond, metal alloys, complex oxide ceramics, and others.

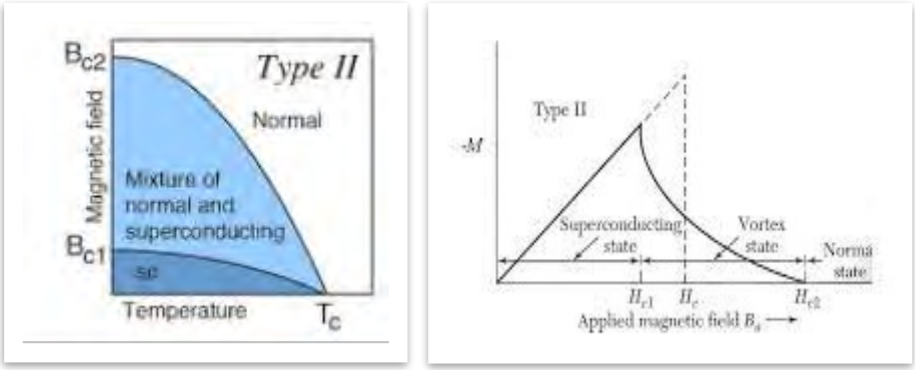

Fig 1.4: (a) Magnetization vs applied magnetic field for type II superconductors.

(b) H-T Phase illustration

1.4 PROPERTIES OF SUPERCONDUCTING MATERIALS:

1.4.1 Meissner's Effect:

The complete expulsion of magnetic field lines from the superconducting material as its temperature decreases below critical temperature is called Meissner effect, see figure 1.5 **[13]**. The material behaves as a diamagnetic state when it becomes a superconductor.

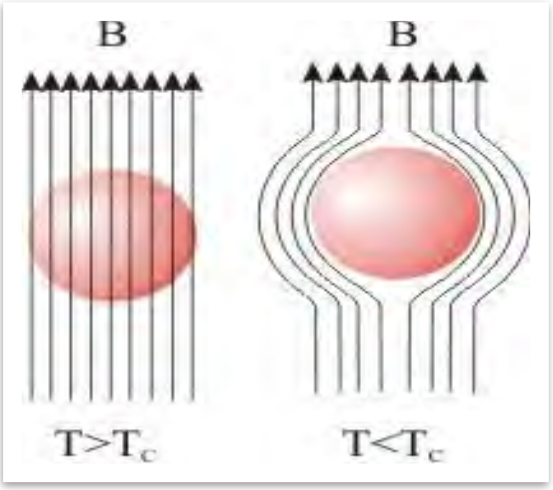

(a) *(b)*

Figure 1.5: Meissner effect; (a) Normal state (b) Superconducting state

Meissner and Ochsenfeld **[14]**, in 1933, observed that their superconducting samples showed diamagnetic behaviour by ejecting the magnetic field lines out of the sample when placed in an external magnetic field**.**

As

$$B = \mu_{\circ} (H + M)$$

As magnetic field disappears inside the superconducting sample, then:

$$M = -H$$

Susceptibility is given as

$$\frac{M}{H} = \chi$$

Here χ = -1, we know that susceptibility for perfect diamagnetic materials is also -1 hence we conclude that superconductors show perfect diamagnetism.

1.4.2 Isotope Effect:

In 1950, it was found that different isotopes of an element have different critical temperatures and this temperature was observed to be inversely proportional to isotope mass i.e.

$$T_c \, M^{\alpha} = \text{constant}$$

Where $\alpha = 0.5$ for most of superconductors and M is the mass of the isotope.

Isotope effect is never said to be a universal phenomenon. Some conventional superconductors do not exhibit isotope effect as shown in Table 1.1.

Material	**α**
Mg	0.5
Sn	0.46
Re	0.4
Mo	0.33
Os	0.21
Ru	0(±0.05)
Zr	0(±0.05)

Table 1.1: Isotope coefficient α of different conventional superconductors

In case of different isotopes of mercury, the critical temperatures were observed to be

Hg (199.5amu) =4.185 K and *Hg* (203.4amu) =4.146 K.

1.4.3 Flux Quantization

In 1961, it was revealed that magnetic flux quantization exists **[15]**. The scientists in Germany and USA separately discovered it at almost same time.

To understand the term flux quantization, first consider a superconducting loop, initially at temperature $T > T_c$, and it is exposed to magnetic field from outside. When temperature of this loop is dropped such that it falls below critical temperature, then the field lines are pushed out of the material pertaining to Meissner effect. Meanwhile, the flux trapped in the loop remains there and it stays there even if the external field is disconnected. It happens when the external field is no longer there, the magnetic flux through the loop first decreases, then due to faradays law of induction, current is induced in the loop, but as now the loop is in superconducting state, the currents continue to flow without losses, and it starts to support the flux. If the ring had some resistance, the current would have decreased and the flux would also have decayed, but in this case, flux takes infinite time to decay, thus appeared to be trapped in a loop as shown in Figure 1.6.

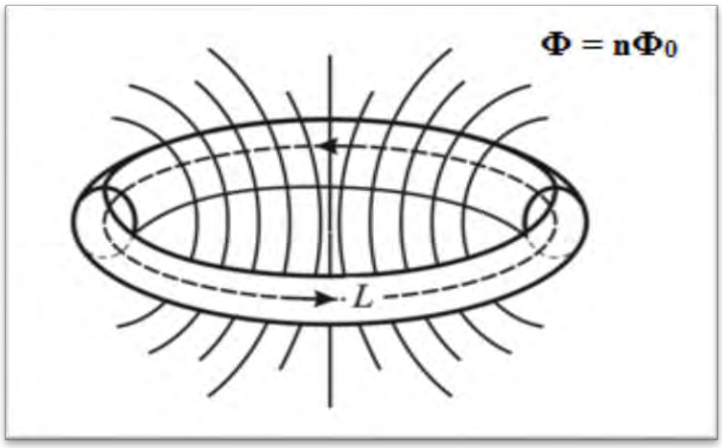

Figure 1.6: Quantization of magnetic flux

The term magnetic flux is defined as the magnetic field times the area of the loop i.e., $\boldsymbol{\Phi = B \cdot A}$. Here Φ can have any value but when we talk about superconducting loop then the flux passing through that loop is always quantized. It means that the flux can only attain certain values. The equation for this term is:

$$\Phi = \frac{2ne}{e^*} \Phi_0$$

Where Φ is total flux trapped in the hole of superconductor and Φ_0 is flux quantum having value $\frac{hc}{2e} = 2.0679$ G cm^2 and e^*=2e (corresponding to cooper pair). This shows that the flux trapped in the hole is quantized **[16]**.

The inverse of the flux quantum is defined as the Josephson constant which is constant of proportionality in Josephson Effect:

$$C_j = 1/\Phi_0$$

1.4.4 The Josephson Effect:

Josephson junction is macroscopic quantum tunnelling phenomena which was observed in 1962 **[17]**. The Josephson Effect is used to obtain measurements with extreme precision of potential difference across the superconducting junction. This tunnelling is observed when two superconductors are joined to each other via a weak link, like small insulating barrier (S-I-S) or a non-superconducting material (S-N-S). The wavefunction of electrons on both sides of the insulating layer interact through this weak link. The cooper pairs tunnel through the barrier and current flows across the junction. For tunnelling of cooper pairs, the barrier length should be very small, that is of the order of nanometre.

There are two types of Josephson effects:

- AC Josephson effect
- DC Josephson effect

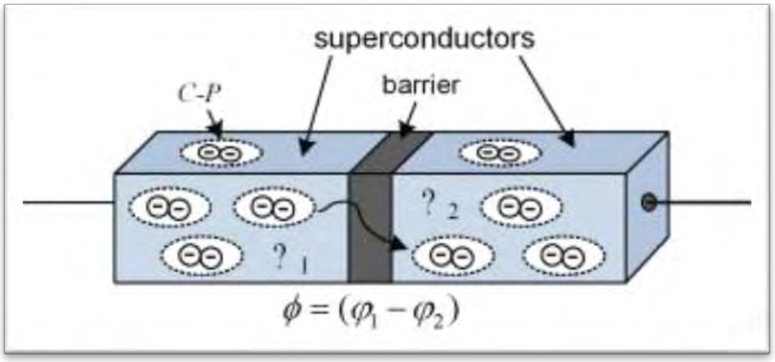

Figure 1.7: Illustration of Josephson Effect

Direct current flows across the weak link in DC Josephson effect without any externally provided voltage. Equation describing DC Josephson effect is:

$$I = I_c sin\theta$$

In AC Josephson effect, an external source of DC voltage is connected to the superconductors which cause the phase change in current flowing through the barrier with time and it is given as:

$$\frac{\partial\theta}{\partial t} = \frac{2e}{\hbar}V$$

The current produced is alternating current and its complete mathematical form is:

$$I_{ext} = C_j \frac{dv}{dt} + I_c \sin\theta + \frac{V}{R}$$

Here C_j is Josephson constant. It relates the frequency of electromagnetic radiation to the potential difference across the Josephson junction. The value of this constant is 4.8×10^{-5} $(GHzV^{-1})$.

In AC Josephson effect, high frequency electromagnetic waves are generated once the value of current surpasses critical.

1.5 DIELECTRIC PROPERTIES OF SUPERCONDUCTOR:

Permittivity is the dielectric property that we analysed in our experiments. It changes in superconducting sample with different factors like temperature, frequency, pressure, and structure of materials.

1.5.1 Capacitor

Capacitor is a device to store electric charge. It consists of two or more layers of conductors separated from each other by an insulator. When a voltage is applied across the plates of capacitor, charges build up and store in it in the form of electrostatic field. The presence of a dielectric between these plates helps to store more charge **[18]**. The capacitance of a capacitor is given as:

$$C = A\frac{\varepsilon}{d}$$

Here ε is the dielectric constant of material. The capacitance is calculated in farad (F).

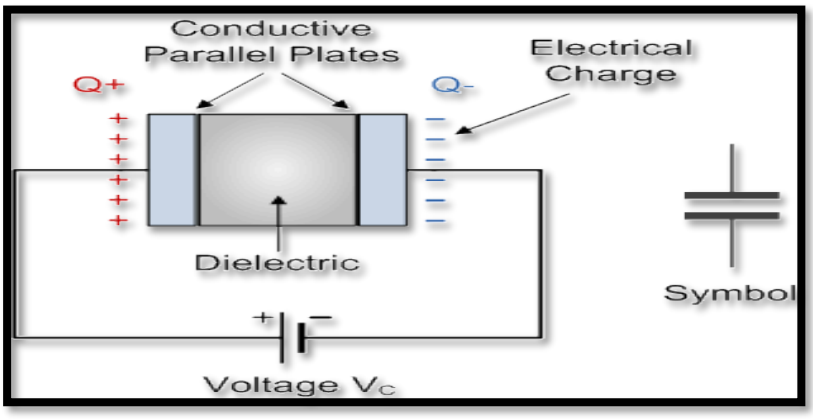

Figure 1.8: Parallel plate capacitor with dielectric

The dielectric constant ε is a complex number with real and imaginary components. Its real part ε′ represents that how much energy is stored due to external field. While its imaginary parts ε″ tells us about the energy lost due to external field.

The ratio of real part and imaginary part of the dielectric constant tells us about the tangent (δ) dielectric loss also known as "dissipation factor".

$$Tan\delta = \varepsilon_r''/\varepsilon_r'$$

1.6 THERMAL PROPERTIES OF SUPERCONDUCTOR:

In normal metals, the free electrons play the role of conduction. These free electrons get scattered by impurities in the material. When it comes to superconductors, there happens to be an ordering among electrons (formation of cooper pairs) which helps to avoid the scattering through these obstacles and thus leads to superconductivity. There are many materials which become superconducting when their temperature is decreased. The transition that happens between normal and superconducting states is experimentally observed to be thermodynamically reversible. Here are some thermal properties of superconductors;

- Entropy
- Heat Capacity
- Free Energy

1.6.1 Entropy

Entropy defines how much a system is disordered. When a material becomes a superconductor, it is observed that its entropy decreases, which shows that the superconducting state is more ordered than the normal state. At T_c, however, both states have same entropy.

Superconductivity is based on cooper pairs behaving coherently. If entropy of superconducting state is S_s and entropy of normal state is S_N, then the difference between these entropies is:

$$S_N - S_S = -\frac{H_c dH_c}{dt}$$

Here H_c is the critical magnetic field.

At $T=T_c$ $H_c = 0$ so $S_N - S_S = 0$

At $T=0K$ again $S_N - S_S = 0$

The image in figure 1.9 depicts the entropy of normal and superconducting states as a function of temperature.

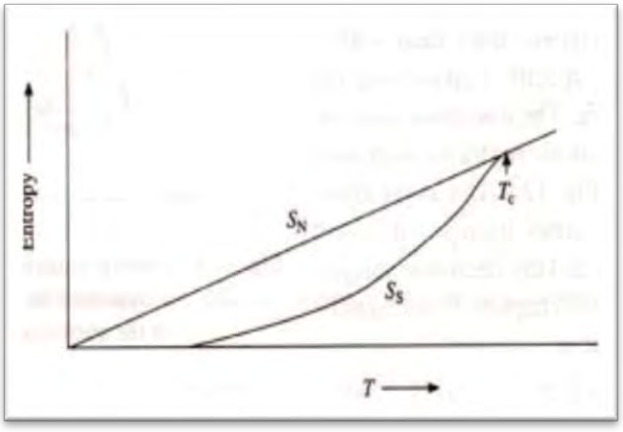

Figure: 1.9: Entropy curves in superconducting state and normal state

1.6.2 Heat Capacity

The temperature dependency of typical metal's heat capacity is given as:

$$C_n(T) = \gamma T + \beta T^3$$

When heat is added in a system, part of it increases electronic specific heat which is represented by the first term. The remaining energy is used to increase the lattice vibrations at low temperature, which is represented by the second term in the above equation. As we know that superconductivity affects electrons for their pairing to form cooper pairs and lattice properties like crystal structure and Debye temperature remains unaffected so specific heat due to lattice vibration remains same in normal and superconducting state. Thus, we will be concerned with electronic heat capacity part here. It is found that electronic heat capacity part varies exponentially with temperature **[20]**.

Where Δ represent energy gap. This energy gap reduces to zero as the temperature falls below the transition point. This is also the reason that electrons in superconductors have a higher specific heat than electrons in ordinary metals as seen in Figure 1.10. But when we increase the temperature above critical temperature of that superconductor, the energy gap again starts to increase. This happens along with the breaking of cooper pairs. To break a pair, energy equal to the energy gap Δ is required for each electron. The total energy required to break a cooper pair will be twice of it i.e., 2Δ.

$$C_{es} = Aexp(\frac{-\Delta}{k_B T})$$

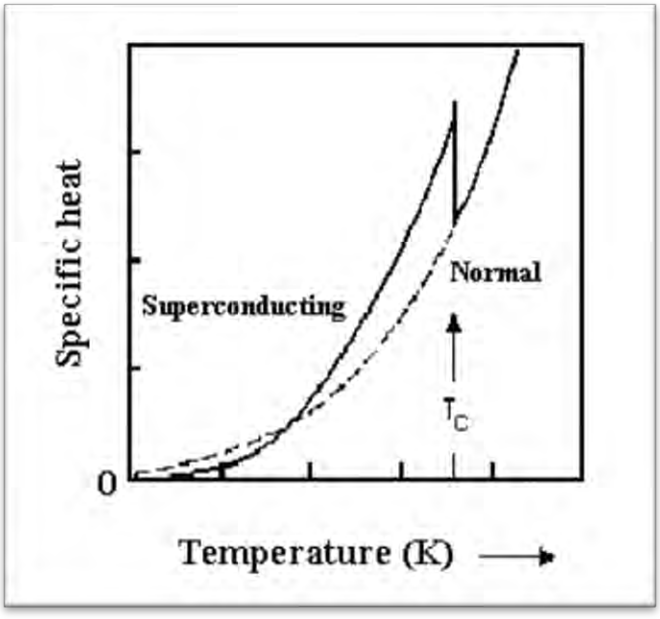

Fig 1.10: Temperature vs heat capacity curves of normal and superconducting states

1.6.3 Free Energy

In superconducting state, the free energy is always less than that of normal state. When g_s (T, H) becomes greater than g_s (T, H) then superconductivity vanishes.

Gibbs free energy is given as;

$$g_s(T, H_a) = g_s(T, 0) + \frac{H_a^2}{2\mu_0} \qquad 1.1$$

Applied magnetic field is represented by H_a. At some temperature, if the magnetic field is applied in such proportion that the normal and superconducting states come in equilibrium then their free energies become equal **[21].**

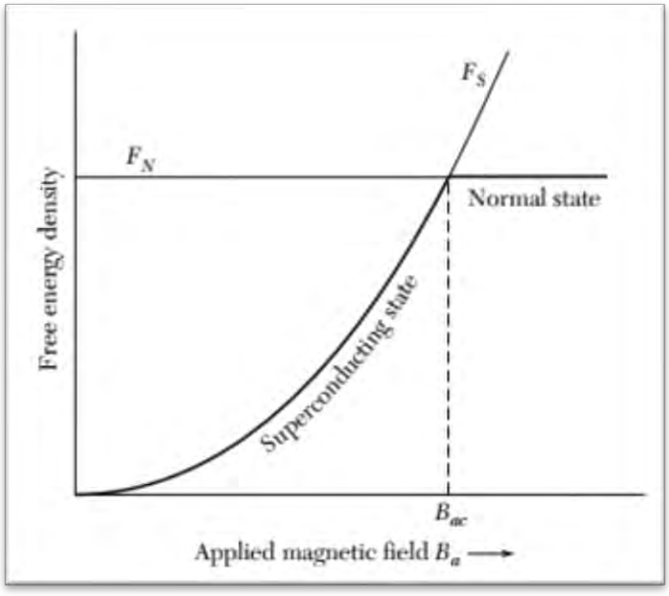

Fig 1.11: Free energy vs Applied Magnetic effect

1.7 BASIC THEORIES OF SUPERCONDUCTIVITY

1.7.1 London Theory

In 1935, two scientists Fritz London and Heinz London purposed a phenomenological theory to explain the electrodynamics of superconductors **[22].** In this theory, two equations are used to explain the electromagnetic field of superconductors in addition to Maxwell's equations. The basic assumption of this theory is same as two fluid model. The behaviour of superconducting electrons is explained by London equations together with Maxwell equations. While the Maxwell equations already described the behaviour of normal electrons. The Meissner's effect is also clearly explained by this theory. To formulate, consider a superconducting sample in an electromagnetic field , and the field is not enough strong to distrub the density of suerconducting electrons. So the density of superconducting electron is uniform. Then the equation of motion of superconducting electrons is given by

$$n_s m \frac{dv_s}{dt} = n_s eE \qquad 1.2$$

Where "n_s" is density of superconducting electrons, "m" is mass of electrons "v_s" is velocity of superconducting electron, "e" is charge of electron and "E" is electric field intensity. We also know that the supercurrent density is given by

$$J_s = n_s ev \qquad 1.3$$

Differentiate equation (1.3) with respective to time 't' and put the value of dv_s/dt into equation (1.2) we get

$$\frac{dJ_s}{dt} = \frac{n_s e^2}{m} E \qquad 1.4$$

This equation is called first london equation which shows that when electric field is zero then there is always a steady state current in superconductor. Now consider Maxwell's equation

$$\nabla \times E = -\frac{\partial B}{\partial t} \qquad 1.5$$

In equation (1.5) when E =0 then there will be a constant magnetic field B inside a superconductor, which contradicts to Miessner's effect. To solve this problem we modify London equation (1.4) and the resultant equation is given by

$$\nabla \times J_s = \frac{n_s e^2}{m} B \qquad 1.6$$

Equation (1.6) is called london second equation which described experimental results succesfully.

1.7.2 Ginzburg-Landau (GL) Theory

The first quantum theory of superconductivity was developed by V. L. Ginsburg and L. D. Landau in 1950 **[23].** Ginzburg-Landau theory was required because the London theory failed to account for quantum phenomena. There were some factors due to which the need of quantum effects was felt. Firstly, the shift from a normal to a superconducting state is referred to as a second-order phase transition. Secondly, it was observed that the superconducting state has lower entropy than the regular state. Ginzburg and L.D. Landau proposed the existence of an order parameter ψ such that:

$$\Psi(T) = 0 \quad ; \text{If} \qquad T > T_c$$

$$\Psi(T) \neq 0 \quad ; \text{If} \qquad T < T_c$$

While formulating the theory, they used normalised form of order parameter which is $|\Psi|^2$. This tells us about the density of superconducting electrons i.e.$|\Psi|^2 = {}^{n_s}/_{2}$. It also tells us about the state of the system. The system will be in superconducting state when $|\Psi(r)|^2 = 1$ and when$|\Psi(r)|^2 = 0$ then the system will exist in normal state.

The expansion of free energy is given as:

$$F = F_n + \alpha|\Psi|^2 + \frac{\beta}{2}|\Psi|^4$$

In the magnetic field's presence, it becomes:

$$F = F_n + \alpha|\Psi|^2 + \frac{\beta}{2}|\Psi|^4 + \frac{1}{2m^*}|(-i\hbar\nabla - 2e^*A)\Psi|^2 + \frac{|B|^2}{2\mu_0}$$

The two generalized equations of GL theory are:

$$\alpha\Psi + \beta|\Psi|^2\Psi + \frac{1}{2m^*}\left(-i\hbar\nabla - \frac{e^*}{c}A\right)^2\Psi = 0$$

$$j_s = -\frac{i\hbar e}{2m^*}(\Psi^*\nabla\Psi - \Psi\nabla\Psi^*) - \frac{2e^2}{mc}|\Psi|^2\mathrm{A}$$

The two characteristic lengths ξ and λ are also defined by GL theory:

$$\xi = \sqrt{\frac{\hbar^2}{2m|\alpha|}}$$

$$\lambda = \sqrt{\frac{m}{4e^2\Psi\mu_0}}$$

The coherence length tells us about length of order parameter or thermal fluctuation and penetration depth λ tells us the penetration of a magnetic field into the superconductor's surface.

1.7.3 Bardeen, Cooper, and Schrieffer Theory

The Scientist Leon cooper suggested the pairing of electrons in 1956. He thought that due to electron- phonon interaction two electrons get a new stable state. It was the main clue toward the correct theory of superconductivity. This new state of paired electrons is referred to as the cooper pair. The energy of coupled electrons in a substance is smaller than the fermi energy. It means that the paired state is a bound state. J. Bardeen, L. Cooper, and R. Schrieffer provided the first microscopic theory of superconductivity in 1957 **[24];** this theory is called the BCS Theory. The mechanisms of superconductivity were successfully explained by this theory. In the BCS Theory of superconductivity, BCS

condensate is generated below T_c in which the electrons having opposite momenta and spin and energies similar to the Fermi energy pair are present. The superconductivity is being led by this BCS condensate.

1.7.3.1 Formation of Cooper Pairs:

BCS theory explains the formation of cooper pairs. It tells us that whenever electrons in superconductors move through the lattice, it causes lattice vibration. At T=0, there are no lattice movements, the only movements occur if the electron interacts with the lattice.

Consider a free electron travelling in a crystal with the wave vector k1. It induces a lattice vibration at some point in time. To put it another way, the electron produces a phonon (It did not exist beforehand and goes into a new state known as k), suppose the wave vector of the produced phonon is q. The law of momentum conservation gives us,

$$k_1 = k' + q$$

$$k2 = k'' + q$$

Another electron k_2 quickly absorbs the phonon q, resulting in the state k'' so, what happened then? Two electrons that were in the states k_1 and k_2 at the time now have states k' and k''. So, we have,

$$k1 + k2 = k' + k''$$

This implies that they were scattered by one another. However, only when two particles encounter, can they be mutually dispersed. As a consequence, we conclude that the process described above represents a functional electron-electron interaction. This results in the formation of cooper pairs, the two electrons with opposite spin. The electrons are spin half particles but when they form cooper pairs, they have zero spin like bosons. Thus, many electrons can reside in same state and follow Bose Einstein statistics.

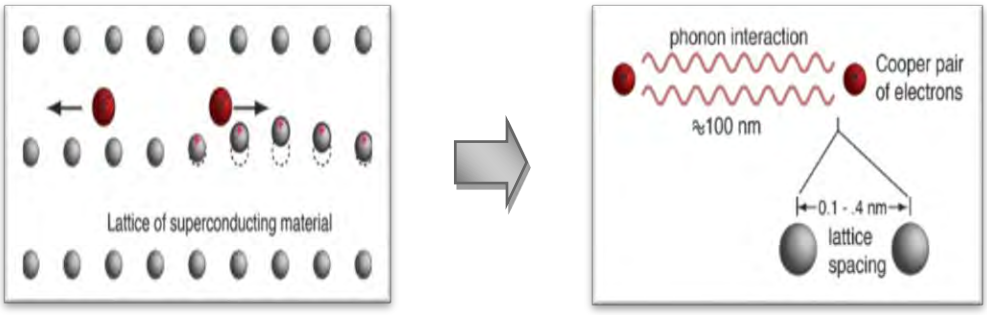

Fig 1.12: Formation of Cooper Pair

1.7.3.2 Coherence Length:

BCS theory defines coherence length as:

$$\xi = \frac{\hbar V_F}{2\Delta}$$

Here V_F is the Fermi velocity and 2Δ is the energy gap.

For type I superconductors: $\xi > \lambda_L$

For type II superconductors: $\xi < \lambda_L$

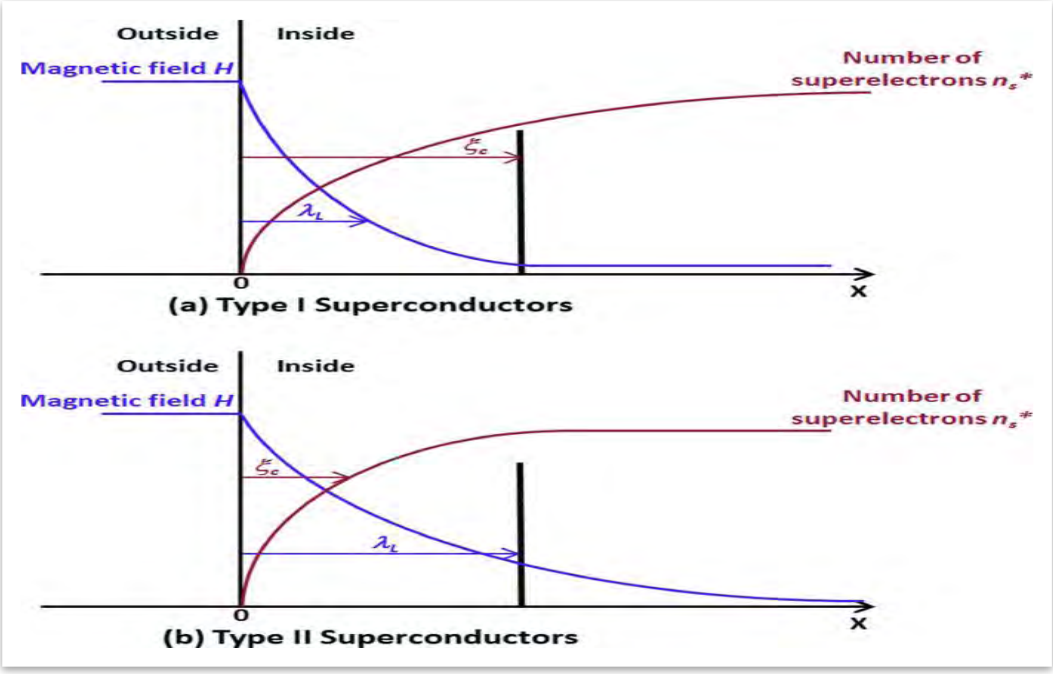

Fig 1.13: Coherence Length in Type I and type II superconductors

1.8 APPLICATIONS OF SUPERCONDUCTORS

Some of the applications of superconductors are given below.

1) On the idea of the zero resistivity, superconductors are used for these subsequent purposes.

- Superconductors can be used in power lines, enabling efficient long-distance transmission, with zero power loss
- Superconducting magnets in electric generators and particle accelerators

2) Using the famous assets of superconductors 'Meissner Effect' superconductors are used for the following functions.

- Magnetic Shielding
- Magnetic resonance imaging (MRI)
- Magnetic levitation trains

3) Based on Josephson impact superconductors have following applications.

- Mineral prospecting
- Magneto cardiogram
- Magnetic flux detectors
- Ultra-rapid computer systems
- Superconducting quantum interference devices shortly known as SQUIDS
- Logic elements
- Non-destructive evolution of computer chips and aircrafts.

1.9 REFERENCES

[1] M. Tinkham, Introduction to Superconductivity, 2004.

[2] W. Meissner, R. Ochsenfeld, Naturwissenschaften 21 (1933) 787–788.

[3] J. Bardeen, L.N. Cooper, J.R. Schrieffer, Phys. Rev. 108 (1957) 1175–1204.

[4] D. van Delft, Phys. C Supercond. 479 (2012) 30–35.

[5] A.D. LS Brizhik, Low Temp. Phys. 104 (1984) 358–366.

[6] P.W. Anderson, Science. 288 (2000) 480–482

[7] Eder, M.H. and G. Gritzner, *Thallium-based cuprate superconductors doped with rare earth oxides.* Superconductor Science and Technology, 2004. **18**(1): p. 87.

[8] Buckel, W. and R. Kleiner, *Superconductivity: fundamentals and applications*. 2008: John Wiley & Sons.

[9] Durajski, A.P., R. Szcze, and Y. Li, *Non-BCS thermodynamic properties of H2S superconductor.* Physica C: Superconductivity and its Applications, 2015. **515**: p. 1-6.

[10] V.L. Ginzburg and L.D. Landau**,** Zh. Eksp. Teor. Fiz 20, (1950) 1064

[11] K. Kotzler, L. Von Sawiski and S. Casalbuoni**,** Phys. Rev. B 64, (2004).

[12] V.V. Schmidt, (Eds) Paul Muller and Alexey V. Ustinov, The Physics of Superconductors, (1997).

[13] W. Meissner, R. Ochsenfeld, Naturwissenschaften 21 (1933) 787–788.

[14] C. Gorter, H. Casimir, Physica 1 (1934) 306–320.

[15] Abrikosov, A. A., Sov. Phys. JETP 5 (1957) 1174–1182.

[16] Doll, R. and M. Näbauer, *Experimental proof of magnetic flux quantization in a superconducting ring.* Physical Review Letters, 1961. **7**(2): p. 51.

[17] B.D. Josephson, Phys. Lett. 1 (1962) 251–253

[18] M.A. Wahab, Solid State Physics, Narosa Publishing House Pvt. Ltd, New Delhi, 2nd edition.

[19] R.K Puri and V.K Babbar, Solid State Physics and Electronics, (1997) 278

[20] S.O. Pillai, Solid State Physics, 5 th edition (2006)

[21] Charles Kittel, Introduction to Solid State Physics, John Wiley & Sons, Inc. 8 th edition (2005)

[22] V. V. Schmidt, P. M. ller, A. V. Ustinov, The Physics of Superconductors : Introduction to Fundamentals and Applications, Springer Berlin Heidelberg, 1997.

[23] V. Ginzburg, On Superconductivity and Superfluidity: A Scientific Autobiography, 2008.

[24] J. Bardeen, L.N. Cooper and J.R. Schrieffer**,** Physical Review 1957. **106**(1): p.162-164.

Chapter 2

LITERATURE REVIEW

In this chapter a concise literature overview of high temperature superconductors (HTSC), Tl-based HTSC, and Zn doped Tl-based HTSC is presented.

2.1 HIGH TEMPERATURE SUPERCONDUCTORS

The empirical elements typically have relatively low transition temperatures. Alloys, such as Nb-Ti and Nb-Al-Ge, typically exhibit transition at relatively high temperatures. In 1986, Bednorz and Muller developed oxide superconductors with T_c ranging from 90 to 125 K **[1].** Following this finding, Paul Chu and his colleagues were able to find 123 ($XBa_2Cu_3O_{7-\delta}$) type oxides with T_c values about 90K **[2].** Researchers were inspired to start an extensive search for novel oxides with higher T_c, superconductors with T_c exceeding the temperature of liquid nitrogen. It was discovered that the T_c ranged from 60K to 125K for the compounds of the Bi-Sr-Ca-Cu-O and Tl-Ba-Ca-Cu-O families **[3].**

2.2 THALLIUM BASED HIGH TEMPERATURE SUPERCONDUCTORS

Because of their high T_c, Tl-Ba-Ca-Cu-O superconductors are regarded as the greatest superconductor family. This group of superconductors have a low microware surface resistance and a reasonably high critical current density. Sheng and Hermann first came to know of this sequence in 1988 **[4].** These superconductors' crystal structures are primarily tetragonal and alternate between single or double Tl-O sheets and perovskite-like Ba-Ca-Cu-O layers **[5]**. The unit cell of one of the members of this family is shown in Figure 2.1

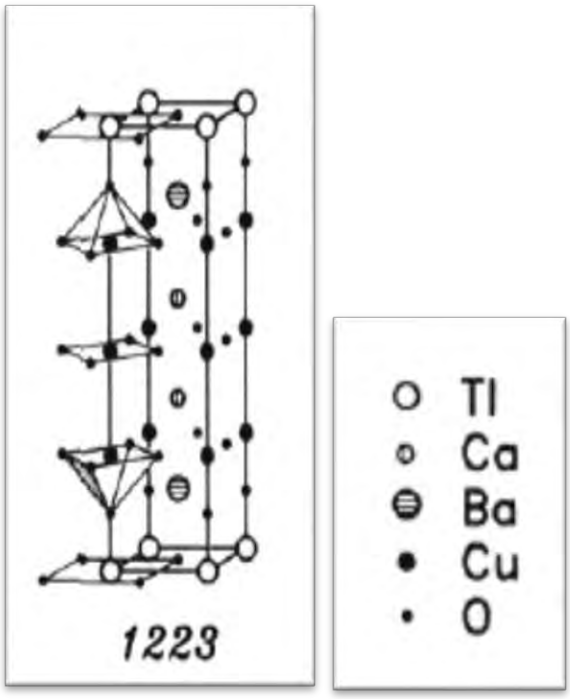

Figure 2.1: Unit cell structure of $Tl_1Ca_2Ba_2Cu_3O_{10-\delta}$

2.3 LITERATURE REVIEW OF Tl-BASED HTSC

Using $Cu_{0.5}Tl_{0.5}Ba_2Ca_2Cu_{3-x}M_xO_{10-\delta}$ (M = Ni, Zn, Cd; x = 0, 1.5) superconducting samples, Nawazish A. Khan et al. **[6]** studied the samples' low-frequency dielectric properties. These superconductors exhibited an orthorhombic structure, and after Zn, Ni, and Cd doping, the size of the a-axis increased while the length of the b and c axes decreased. T_c(onset) and T_c(offset) values decreased when the compound was doped with cadmium, but they increased after Zn and Ni were added. The apical oxygen modes moved after doping, but the peaks corresponding to other vibrational modes remained stationary. They discovered that while the absolute values of these parameters grew as the applied temperature fell, the real and imaginary components of the dielectric constant decreased with frequency. They observed a decrease in values of the two components of dielectric constant when Zinc, cadmium, and nickel were doped as the unit cell's replacement. Cd-doped samples saw the greatest suppression. They proposed that the creation of an-harmonic oscillations in layers was responsible for the decline in the number of Cooper pairs, which in turn fostered a decline in both dielectric constants. In the frequency range, 800 Hz to 1 kHz, they also detected a shift in the value of tan from negative to positive. The beginning of interfacial polarisation caused this transformation. (AC-conductivity) enhnced in samples doped with zinc, nickel, and cadmium, but remained constant in blends.

It showed the formation of anharmonic vibrations and the implications of the breaking of cooper pairs.

M. Raheem et al. **[7]** examined the $Cu_{0.5}Tl_{0.5}Ba_2Ca_3(Cu_{4-x}Cd_x)O_{12-\delta}$ (x= 0, 0.25, 0.5, 0.75) samples to determine the effects of Cd doping at the Cu site. They synthesised their samples using a two-step solid state technique before pelletizing them. They examined the sample's structure using an X-ray diffractometer, measured resistivity using the four-probe method, ac susceptibility using a mutual inductance method, the sample's dielectric properties using an LCR metre. Their sample showed a tetragonal structure with an increasing c axis length as doping of Cd increased, according to the results of the XRD analysis. The zero-resistivity critical temperature is determined by the damped harmonic oscillation of a Cd atom with a mass greater than that of Cu in CuO_2 planes. With increasing Cd content, the zero-resistance critical temperature dropped. This results in a limited population of electron phonon interactions, which diminishes the properties of superconductivity. The actual component of the dielectric constant displayed negative values as a result of negative capacitance, and it continuously decreased with applied frequencies at all temperatures. The actual part of the dielectric constant dropped in magnitude because the polarisation density of heavier Cd atoms reduced due to an-harmonic oscillation. The imaginary fraction of their sample displayed a decreasing trend with increasing frequency and temperature. The tan losses show increasing values with temperature in every Cd doped sample. The reduced losses in Cd doped samples demonstrated the presence of Cd atoms close to faults and grain boundaries. As temperature dropped, a smaller cross section of charge carriers was represented by ac conductivity ratings that decreased. The Cd doped sample's lower ac conductivity values pointed to a dwindling population of electron phonon interactions.

Muhammad Usman Muzaffar et al. **[8]** conducted research and developed a modified synthesis method for $Cu_{0.5}Tl_{0.5}Ba_2Ca_3Cu_4O_{12-y}$ superconductor. A pure $Cu_{0.5}Tl_{0.5}Ba_2Ca_3Cu_4O_{12-y}$ superconducting phase is attained at a normal pressure using this modified approach. Sr is substituted at the Ba site in $Cu_{0.5}Tl_{0.5} - 1234$ sample with concentrations of 0, 0.15, 0.25, and 0.35, which also changes the charge reservoir layer. The substitution of small-sized Sr causes the c-axis lattice parameter to drop, which may result in increased interlayer coupling strength. Infrared spectroscopy using the Fourier transform further supports the Sr replacement at the Ba location. As Sr content increases

up to x = 0.25, the threshold temperature for superconductivity decreases till x = 0.35. According to Aslamazov-Larkin and Lawrance-Donaich's examination of excess conductivity, With the increase in Sr content, the crucial region-3D, 3D-2D, and 2D-SWF crossover temperatures are pushed to lower temperatures; the same is true for the c-axis coherence length. However, as Sr content increases up to x = 0.35, the interlayer coupling strength increases, indicating that the smaller Sr at the Ba site has improved interlayer coupling. The examination of fluctuations-induced conductivity also yields an inverse relationship between c-axis coherence length and the critical temperature.

The $TlBa_2Ca_2Cu_3O_x(Tl-1223)$ superconductors were created as thin films by L. Perez et al. **[9]** and their unique characteristics were investigated. They prepared these samples using a two-step technique. They used different thallium (Tl) diffusion conditions at 550^0C in a two-zone furnace. They preserve films of $TlBa_2Ca_2Cu_3O_x$ (Tl-1223) using spray pyrolysis methods. The thallium diffusion procedure was used to include Tl in the film. They used Tl_2O_3 pellets heated to 750^0C as the source of thallium. They used various oxygen flow rates at atmospheric pressure to obtain thallous oxide (Tl_2O) and obtained films of the Tl-1223 phase with the c-axis perpendicular to the substrate's surface. They came to the conclusion that Tl-1223 and $BaCuO_2$ phases were mixed together in the films. For a thallous oxide pressure of 1.4 x 10^{-2} atm, they obtained crystalline grains with longest sides that had the best superconducting behaviour. The T_c values for these films ranged from 90 K to 102 K.

M. Irfan et al. **[10]** investigated Ge-doped $(Cu_{0.5}Tl_{0.5})$ Ba_2Ca_3 $(Cu_{4-y}Ge_y)$ O_{12-x} (y = 0, 0.3, 0.6, 0.9) samples. At the standard pressure, the synthesis was carried out using the solid state reaction method. XRD analysis, dc-resistivity measurements, FTIR spectroscopy, and ac-susceptibility measurements were used to characterise the samples. They discovered that the samples had P4mm space group tetragonal crystal structure. They observed that T_c reduced as Ge concentration increased. The localization of carriers at Ge^{4+} particles is what causes the T_c to fall. The scientists observed that after post-annealing the samples, T_c and the diamagnetic properties were both enhanced. FTIR absorption spectra were used to investigate the phonon modes. Additionally, they observed that the planer and apical oxygen phonon modes have been relocated so that they are no longer in the way of the replacement of Ge at Cu planer sites. For these samples, the phonon modes connected to O remain unchanged.

P. Chaddah et al. **[11]** investigated the magnetic properties and critical state model of high T_c superconductors in 1989. To comprehend the magnetic behaviour of high critical temperature superconductors, they introduced the critical state model. They noticed that as magnetic field values increase, the critical current density values decrease drastically. Isothermal magnetization curves of these samples showed characteristics related to the intra and inter-granular regimes of sintered pellets with high critical temperatures of superconducting material. While sintered pellets were tested by inter-granular sections, single crystal transport predictions of critical current density were measured using intra-granular regions.

A.l. Abou-Aly et al. **[12]** studied the thermal fluctuations of synthetic superconductors $Tl_{0.8}Hg_{0.2}Ba_2Ca_{2-n}R_nCu_3O_{9-y}$ R = Yb, Sn;(n= 0-0.15) above the transition temperature. Although (Tl, Hg)-1223 was the predominant phase in these samples, an x-ray diffractometer also detected impurities. They used the four-probe method to measure resistivity and the Aslamazov-Larkin equations to conduct conductivity analysis. The important regime, 3D, 2D, 1D, and short wave zones of thermal fluctuations were highlighted after this examination. The 1D regime of oscillations in (Tl, Hg)-1223 caused conducting charge belts to exist in the samples. Sample doping increased the inter-grain coupling while decreasing the coherence length. The critical current density and magnetic field values (B_{c2}, B_c, B_{c1}) decreased after the dopant was added. After doping, the unit cell of superconducting samples shrunk, increasing Fermi energy.

By the doping of Zn at Cu site, Rishi Kumar Singhal et al. **[13]** were able to explain the magnetic characteristics of the YBaCuO-123 sample. They created polycrystalline materials [$YBa_2(Cu1\text{-}xZnx)_3O_7$; x= 0, 0.02, 0.04, 0.06] using a solid-state reaction technique and compounds named Y_2O_3, $BaCO_3$, CuO, and ZnO. They properly combined these compounds in line with the sample's chemical composition. They carefully fired the sample three times at 9500 ^oC in a preheated furnace. They used a lot of intermediate grindings to get the required uniformity. They are currently palletizing the sample and annealing it in an environment of oxygen. To characterise the sample, they used the XRD analysis, resistivity, AC susceptibility, and oxygen stoichiometry techniques. The XRD analysis showed that these samples have orthorhombic structure. The extraordinary diamagnetism behaviour of the samples is examined by the AC susceptibility. They proved that Zn cation has replaced Cu in the planer sites in these samples. Since zinc cation is used

as a deeply solid scattering location, this replacement results in the distortion of the crystal's lattice, activating the nearby magnetic moments. Due to the altered oxygen level, the hole density reduced and the sample's critical temperature eventually dropped. The AG pair breaking theory states that pair breaking plays a crucial role in hiding the wonder of superconductivity.

The high-pressure synthesis of $TlBa_2Ca_{x-1}Cu_xO_y$ (x = 3, 4) superconductors was investigated by A. Iyo et al. **[14].** They investigated the samples' XRD, composition analysis, and susceptibility measurements. They found that there are numerous circumstances that can raise the T_c of the Tl-1223 superconductor. It was discovered that the higher pressure condition significantly increased T_c. It was also investigated how accidentally added carbon from the beginning molecule ended up in the samples. They noticed the position and concentration of carbon in the lattice of the Tl-1223 sample were not known with certainty. Residual carbon would get into the thallium site, lowering the concentration of holes in the CuO_2 planes and interfering with the creation of the optimum composition. The T_c of the Tl-1234 system was also found to be improved by the decreased Tl concentrations. Additionally, they discovered that lower thallium concentrations are beneficial at raising T_c because they prevent Tl from substituting for Ba and Ca sites. In their research, they discovered that the $TlBa_2Ca_{n-1}Cu_nO_y$ maximum T_c is approximately 133.5K for n=3 and 127K for n=4. The researchers discovered that the T_c of the Tl-1223 and Tl-1234 systems are similar to those of the Hg-1223 sample. T_c is more than 130K in the Hg-1223 sample because Hg did not replace the Ba and Ca sites, whereas Tl-1223 uses Tl to partially replace the Ba and Ca sites. They showed that under high pressure and low residual carbon concentration, replacement of Tl at the Ba and Ca sites is significantly reduced. They discovered that the concentration of residual carbon, synthesis temperature, and thallium content all have a substantial impact on the samples' ability to increase T_c and their overall superconducting properties. The authors came to the conclusion that samples needed to be manufactured at high pressure using precursor with little residual carbon in the starting compounds in order to prevent the substitution of Tl.

2.4 ZN DOPED Tl-BASED HTSC

B. S. Yadav et al. **[15]** using a conventional ceramic technique, bulk superconducting samples of the $Tl_2Ba_2Ca_{n-1}Cu_{n-x}Zn_xO_8$ type were synthesized (where n = 2, 3 and x = 0, 0.1, 0.25, and 0.50). Using the powder X-ray diffraction technique, the synthesised materials'

general structural properties and phase identification were determined. Transmission and scanning electron microscopy were used to examine the micro-structural properties of these materials. Energy dispersive analysis of X-rays was used to determine the chemical compositions of these materials. The lattice parameter "c" varied while "a" showed no regular fluctuation, according to the powder X-ray diffraction patterns, however the bulk structure of Tl-2212 and Tl-2223 remained tetragonal with Zn substitution up to 0.50. As x increased from 0 to 0.50, the transition temperature (T_c) was measured and it decreased.

As a potential difference of 1 V/cm occurred across the sample by increasing current, the transport critical density (J_c) values were also determined using the conventional four-probe method. The structural aspects of the superconductors are improved by the electron microscopic studies, such as the transport critical current density "J_c" and stacking faults and uniform ZnO nanoparticle distribution. Due to the homogeneous distribution of ZnO nanoparticles, which serve as flux pinning centres, the observed increase in transport critical current densities (J_c) of at least one order of magnitude can be attributed to this.

By using a solid-state reaction technique Indu Verma et al. **[16]** synthesised samples of $(Bi,Pb)_2Sr_2Ca_2Cu_{3-x}Zn_xO_{10+y}$ (Bi-2223, x=0.00 to 0.30). These compounds were thoroughly synthesised, and then they performed phase formation, structural/microstructural, electrical, and magnetic experiments on them. All the samples were crystallised in an orthorhombic structure with lattice parameters of a = 0.5405 nm, b = 0.5422 nm, and c = 3.7063 nm up to Zn concentration of x = 0.30, according to the phase identification characteristics of synthesised HTSC samples observed using a powder x-ray diffraction technique. The critical temperature (T_c) was shown to decrease from 108 K to 92 K using the conventional four-probe method, and the transport current density, J_C , enhanced as the Zn content (x) climbed from 0.00 to 0.30. SEM and AFM (atomic force microscopy and scanning electron microscopy) surface morphology/topography research showed that the Zn concentration increases along with the size and porosity of the grains, voids, and microsphere/nanosphere-like structures on the surface of the Zn doped Bi-2223 sample. The lower (H_{c1}) and upper (H_{c2}) critical magnetic fields were measured at 10 K from the M-H loop, respectively, from the magnetic properties measurement (M-H).

Markus_Kühberger et al. **[17]** synthesized samples $(Tl_{0.5}Pb_{0.5})(Sr_{0.9}Ba_{0.1})_2Ca_2(Cu_{1-x}Zn_x)_3O_8$) with the concentration of Zn (x= 0, 0.01, 0.05, 0.1) to evaluate the effect of Zn doping on the physical and electrical properties of the Tl-1223 phase. Malic acid gels were

used to generate precursor materials containing Sr-Ba-Ca-Cu-Zn, which were then subjected to a 900°C calcination process. By co-milling, Tl_2O_3 and PbO were added. Superconducting material of excellent quality was produced by sintering in an oxygen atmosphere. The electrical characteristics were improved by oxygen annealing, re-grinding, and re-sintering, which resulted in critical temperatures $T_c(0)$ of 117 K and critical current densities as high as 3800 A cm^2 at 77 K for bulk phase material. The inclusion of Zn modified the microstructure, somewhat lowered the transition temperature and decreased the critical current density at 77 K while also increasing the content of Tl-1212 phase.

2.5 REFERENCES

[1]Bednorz, J.G. and K.A. Müller, *Possible highT c superconductivity in the Ba− La− Cu− O system.* Zeitschrift für Physik B Condensed Matter, 1986. **64**(2): p. 189-193.

[2] Parmigiani, F., et al., Observation of carboxylic groups in the lattice of sintered Ba 2 Y Cu 3 O 7− y high-T c superconductors. Physical Review B, 1987. **36**(13): p. 7148.

[3] Sheng, Z. and A. Hermann, Superconductivity in the rare-earth-free Tl–Ba–Cu–O system above liquid-nitrogen temperature. Nature, 1988. **332**(6159): p. 55-58.

[4] Hazen, R., et al., *100-K superconducting phases in the Tl-Ca-Ba-Cu-O system.* Physical review letters, 1988. **60**(16): p. 1657.

[5] Parkin, S., et al., Tl 1 Ca n− 1 Ba 2 Cu n O 2 n+ 3 (n= 1, 2, 3): A New Class of Crystal Structures Exhibiting Volume Superconductivity at up to≃ 110 K. Physical review letters, 1988. **61**(6): p. 750.

[6] Nawazish A. Khan, Aisha Saba and Asad Raza, Journal of Alloys and Compounds 757, 476-483 (2018).

[7] M. Rahim, N.A. Khan, M. Mumtaz, J. Low Temp. Phys. 172 (2013) 47–58

[8] Muzaffar, M.U., et al., Modified synthesis route to achieve Sr substituted $Cu_{0.5}Tl0_{.5}$-1234 superconductor phase. Materials Chemistry and Physics, 2016. **181**: p. 384-390.

[9] Pérez-Arrieta, L., et al., Two step synthesis of $TlBa_2Ca_2Cu_3O_x$ films on Ag substrates by spray pyrolysis of metal-acetylacetonates. Revista mexicana de física, 2008. **54**(6): p. 446 450.

[10] Irfan, M. and N.A. Khan, How ge Doping Affects the Superconducting Properties of (Cu, Tl)-1234 Superconductors. International Journal of Modern Physics B, 2011. **25**(29): p. 3853-3861.

[11] Chaddah, P., et al., Critical state model and the magnetic behaviour of high Tc superconductors. Cryogenics, 1989. **29**(9): p. 907-914.

[12] A.l. Abou-Aly, R. Awad, I.H. Ibrahim and W. Abdeen, Solid State Communications 149, 281 (2013)

[13] Singhal, R.K., How the substitution of Zn for Cu destroys superconductivity in YBCO system, Journal of alloys and compounds, 2010. **495**(1): p. 1-6.

[14] Iyo, A., et al., High-pressure synthesis of $TlBa_2Ca_n - 1Cu_nO_y$ (n= 3 and 4) with Tc= 133.5 K (n= 3) and 127 K (n= 4). Physics C: Superconductivity, 2001. **357**: p. 324-328.

[15] Yadav, B. S., Verma, G. D., Phase, D. M., Lalla, N. P., & Das, B. SYNTHESIS AND STRUCTURAL/MICROSTRUCTURAL CHARACTERISTICS OF Zn-DOPED Tl-BASED HIGH-Tc SUPERCONDUCTORS. *International Journal of Modern Physics B*, 2011. **25**(27): p. 3583-3594.

[16] Verma, I., & Nidhi Verma, R. Studies on physical properties of nanostructured ZnO doped Bi-2223 superconductors. *Advanced Materials Letters*, 2012. **3**(3), 250-254.

[17]Kühberger, M., & Gritzner, G. The influence of zinc on Tl-1223 superconductors. *Physica C: Superconductivity*, 2003. **390**(3), 263-269.

Chapter 3

SYNTHESIS AND EXPERIMENTAL TECHNIQUES

In this chapter we will briefly go into the synthesis of thallium-based Zn-doped CuTl-1223 superconductors. We will also go through the methods used to characterise these materials. These methods include DC resistivity measurement, XRD (X-ray diffraction), FTIR (Fourier transform infrared spectroscopy), and FIC (fluctuation induced conductivity analysis).

3.1 SYNTHESIS:

The two step solid state reaction method was used for the synthesis of $Cu_{0.5}Tl_{o.5}Ba_2Ca_2Cu_3O_{10-\delta}$ and series $Cu_{0.5}Tl_{o.5}Ba_2Ca_2Cu_{3-x}Zn_xO_{10-\delta}$ where x=1, 2, 3. The compounds used here were CuCN, $Ba(NO_3)_2$, $CaCO_3$, and Tl_2O_3, for zinc doping ZnO was used. The required compound was ground for one hour in mortar and pestle. The grounded material was then loaded in quartz boat and then it was placed in the pre heated furnace at 860^{o}C for 24 hours.

The sample was cooled to room temperature after 24 hours. The material was then milled for an additional hour before being re-inserted into the furnace for a further 24 hours in alumina boats. The thallium is added to the precursor $Cu_{0.5}Tl_{o.5}Ba_2Ca_2Cu_3O_{10-\delta}$ after it has already been made, and the mixture is then again crushed for an additional hour. Following that, the material is palletized using 3.8 tons/cm^2 of pressure. The pallets are then wrapped in gold foil and sintered in a furnace for twelve minutes. At room temperature, it is subsequently cooled. During sintering, the gold capsule stops thallium from being lost.

The same method was used to create $Cu_{0.5}Tl_{o.5}Ba_2Ca_2Cu_{3-x}Zn_xO_{10-\delta}$ where x=1, 2, 3 and ZnO compound was added as necessary. Finally, we successfully obtain the four samples. For further characterization, the produced samples are subsequently coated with butter paper and then aluminium foil.

3.2 TECHNIQUES FOR CHARACTERIZATION OF THE SAMPLE:

Following are the techniques used to characterize synthesized samples:

- X-Ray diffraction
- DC- resistivity measurement
- FTIR
- FIC analysis

3.3 X-RAY DIFFRACTION TECHNIQUE:

The X-ray diffraction (XRD) method is employed to obtain details regarding the material's crystal structure. This study is performed to determine the cell characteristics of the crystal lattice and to determine if the material is crystalline or not **[1].** Knowing the material's crystal structure is the XRD's most important feature. Prior to the discovery of X-Ray, there was no experimental evidence to support the notion that the atoms of a solid are ordered periodically. Scientists are now in a better position to properly observe the material's structure thanks to the X-ray's discovery.

X-rays are extremely high energy beams with a wavelength of 0.5 to 2.5 that is similar to the distance between atomic layers in materials. Transitions from the K-shell result in the production of X-rays. K-shell X-rays are used to investigate the structure of crystals since they have a shorter wavelength than X-rays from the L or M shells. Because Cu and Mo produce intense beams with wavelengths of 0.8 and 1.5, respectively, these two X-ray sources are most frequently utilised as X-ray sources **[2, 3].**

Any crystal consists of parallel planes and the necessary condition for the diffraction of x-rays from the crystal is that, the distance covered by two parallel beams of X-rays is integral multiple of its wavelength used. This condition is known as Bragg’s law. Schematically diffraction of X-rays from two sets of parallel planes is shown in Figure 3.1.

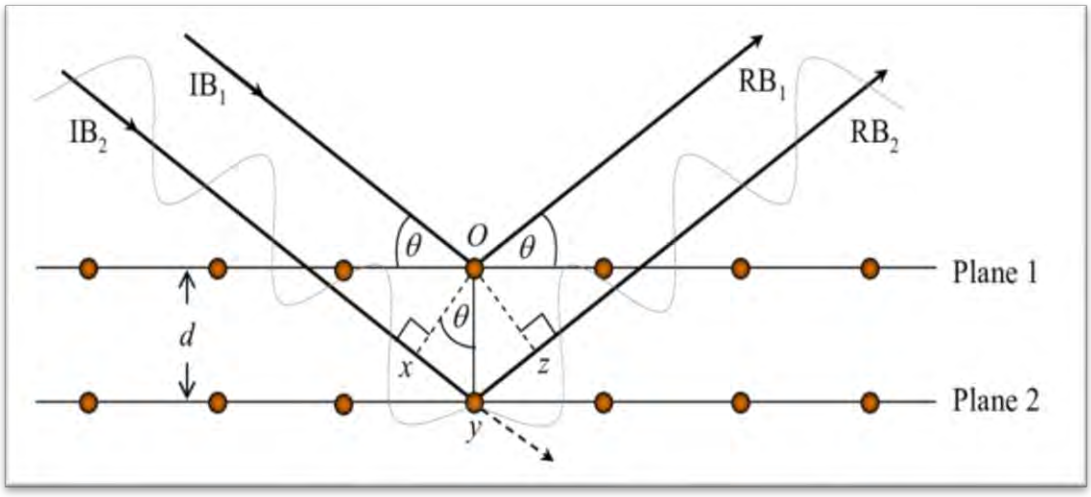

Figure 3.1: X-Ray diffraction from a crystal lattice

The path difference between two parallel x-rays is given by

$$xy + yz = Path\ difference \qquad 3.1$$

According to Bragg's law, for constructive interference this path difference equals the integral multiple of wavelength used.

$$xy + yz = n\lambda \qquad 3.2$$

From Figure 3.1

$$xy = yz = d\ sin\,\theta \qquad 3.3$$

So

$$2d\ sin\,\theta = n\lambda \qquad 3.4$$

where 'd' is the interplanar spacing, 'θ' is the diffraction angle, 'n' is positive integer, and 'λ' is the wavelength of X-rays. Eq 3.4 is the mathematical form of Bragg's law **[4].**

Normally, the following three methods are commonly used for the diffraction of X-rays from crystal.

• Laue method

• Rotating-crystal method

• Powder method

XRD analysis is one of the most important techniques to study the structure of materials. After the synthesis of samples, we performed XRD analysis of these samples. We used D8 Focus, Bruker model XRD machine which works on powder diffraction method. Cu is used as X-rays source with k_α lines having wavelength of *1.5406 Å*. The range of '*2θ*' used is 4–60°. The scan speed fixed at 0.8 sec/step. The diffraction data is collected on a computer system.

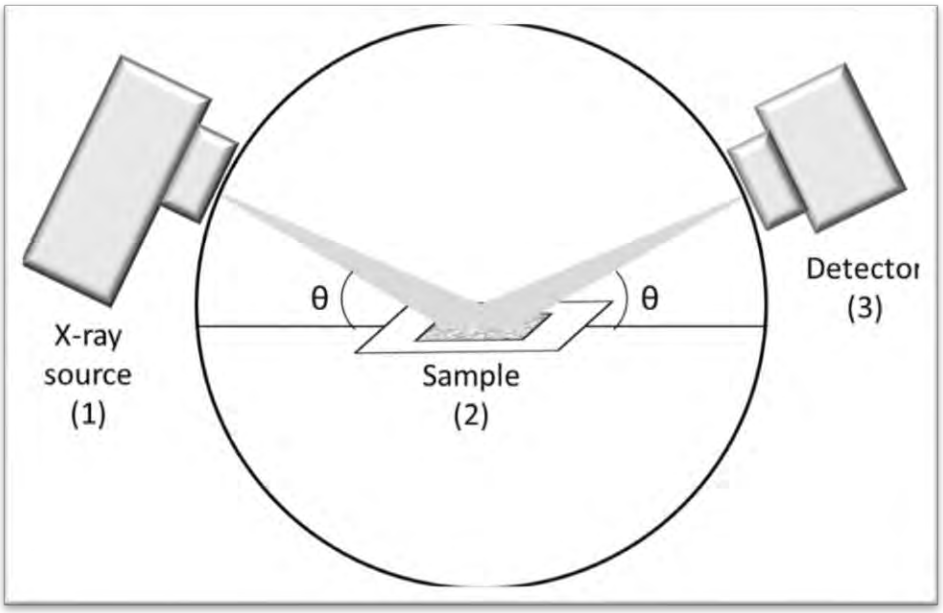

Figure 3.2: Schematic illustration of XRD

Using Chekcell software, the structural data is recovered from the data. It provides details regarding the lattice parameters a, b, and c. The volume of a unit call is determined using the values of a, b, and c. Finally, the graphs are plotted using origin software, and the hkl values are noted on the corresponding peaks. The crystallite size of the samples is calculated using Debye-Scherrer equation **[5].**

$$D = \frac{k\lambda}{\beta cos\theta}$$

Where k is 0.9, λ is 1.5406 Å, θ is the angle of diffraction, β is full width at half maxima.

3.3.1 Advantages and Disadvantages of XRD:

Following are some XRD benefits and drawbacks:

• X-ray diffraction is a widely utilised technique.

• X-ray diffraction is a practical and affordable method.

• The sample does not need to be placed in a vacuum because air does not readily absorb X-rays.

• X-ray diffraction is a quick, simple, and less harmful method.

• Photographic film is capable of detecting X-rays.

In addition, X-rays are unable to differentiate between various isotopes of the same element and are unable to interact significantly with lighter atoms.

Using Debye-Scherrer equation the crystallite size of the samples is calculated.

3.4 DC RESISTIVITY MEASUREMENT

DC resistivity measurements are used to look at a sample's electric properties. Like in a conductor, free electrons can travel in any direction. But once voltage was applied, they were ready, motion began in only one direction, and a current was produced across the wire. Defects, phonons, and the lattice of a conductor prevent electrons from moving freely, increasing resistance (R). V=IR is derived from Ohm's law.

Here, the letters "I," "V," and "R" stand for the conductor's current, electrical voltage, and conductor resistance, respectively.

In other words, a conductor's resistance is inversely proportional to the size of its cross-section (A) and directly proportional to its length (L) as follows:

$$R = \frac{\rho L}{A}$$

Here, "ρ" is a function of temperature and is known as the conductor's resistivity.

$$\rho(T) = R(T)\frac{A}{L}$$

$$R(T) = \rho(T)\frac{L}{A}$$

As Ohm's Law says

$$R(T) = \frac{V}{I}$$

$$\rho(T) = \frac{V}{I}\frac{A}{L}$$

The unit "Ω-cm" is used to measure resistivity. The effects of temperature (T) and average collision time (τ) on electrical resistivity are significant. According to Matthiessen's rule, the sum of three separate causes determines a material's overall resistivity.

$$\rho = \rho_{phonon} + \rho_{defect} + \rho_{impurity} + \rho_{boundary} \qquad 3.5$$

The final three components in equation (3.5) are defined together as residual resistivity (ρ_{res}), which is independent of temperature. However, the first term in equation (3.5) depends on temperature **[6].** For instance, phonons on the order of T^5 are what cause the resistivity dependency on temperature in alkali metals. Due to dispersion from phonons and lattice imperfections, electrical resistivity is dependent on average time (impurities).

The probability of scattering is determined by;

$$1/\tau = 1/\tau_{ph} + 1/\tau_i \qquad 3.6$$

The samples' DC resistivity was evaluated using the Four Probe method. Four-probe approach is preferred for precise measurements in order to eliminate these influences. The prepared sample's shape or form has an impact on the measurements of resistivity **[7].** This technique is commonly used to determine the resistivity of metals, semiconductors,

synthetic polymers and superconductors. During this process, four contacts are bound to the superconducting sample's surface, and these connections are created using silver paste. Silver paste is preferred for excellent contacts that do not crack when the sample is cooled. This method uses two different lead pairs to measure the current and voltage values. A concept is shown in the Figure 3.3.

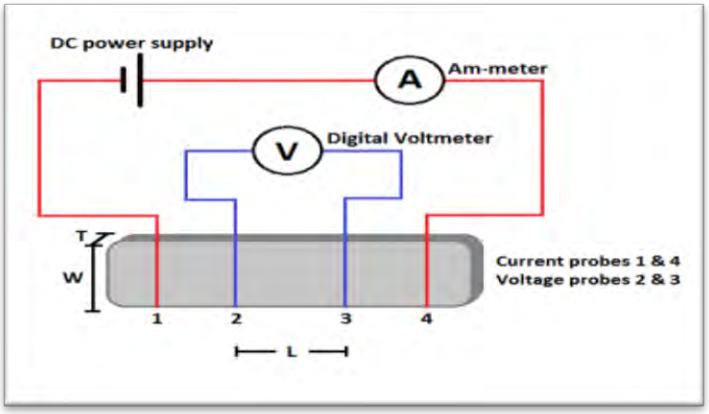

Fig 3.3: Schematic Illustration of four-probe technique

While the inner two contacts transmit voltage drop across the superconducting sample, the outside two connections carry current "I" through it. This method can be used to measure the voltage drop between probes "1" and "2," the current "I" flowing through contacts "3" and "4", the distance between probes "1" and "2," and the cross-sectional area "A" of the sample. A current of roughly 1mA is used to assess resistivity, and the voltage is recorded for each temperature range between ambient temperature and liquid nitrogen where the sample is kept. Making a thermocouple that measures temperature in mV allows one to calculate the sample's temperature. Liquid nitrogen is used to chill the sample since superconductivity only occurs below room temperature. A list of resistance values corresponding to a temperature value is produced by this method. The resistivity can be measured if the resistance value is known. This method enables us to plot a graph between resistance and temperature that indicates whether or not a superconductor has formed. The superconductor has been successfully created if the graph indicates a sudden transition.

3.5 FOURIER TRANSFORM INFRARED SPECTROSCOPY (FTIR)

FTIR is a useful method when dealing with samples' optical characteristics. The atoms in the lattice maintain their oscillation about their mean sites despite the fact that this vibrational motion does not exist in materials at absolute zero temperature. The behaviour

of these phonons (vibrations) determines the mass of the lattice atoms, the distances between them and other atoms, as well as the bond angles between them. These factors collectively determine how phonons (vibrations) differ in solids.

The related energy for these anomalous phonons, when taken into consideration up to the level of quantum mechanics, is equivalent to the energy of a straightforward harmonic oscillator, which is given as;

$$E = \left(n + \frac{1}{2}\right)\hbar\omega_0 \quad \text{for n= 0,1,2,3...} \qquad 3.7$$

Here, the Planck constant is written in a modified form, with "$\hbar$" standing for the oscillator's angular frequency and = h/2, or 1.054x 10^{-34} Js. Since the energy statement E_0 = 1/2 implies that the ground state possesses energy as well, we insert n=0 in the equation (3.7) to calculate its energy. They are crucial in describing the optical properties of the treated samples. Fundamentally, an in-depth knowledge of vibrational modes aids in characterising solid materials (samples), and it is crucial to identify the specific type of vibrational modes present in prepared samples. FTIR spectroscopy is the practice of investigating vibrational modes using a Fourier transform infrared radiation (FTIR) spectrometer.

Fig 3.4: Experimental Apparatus of FTIR

Lattice vibrations and IR radiations have similar frequencies, hence when utilising the FTIR technique, IR radiations are favoured. Resonance-induced absorption peaks can be visible in the FTIR spectrum when their frequencies match. However, resonance won't take place if the condition of matching frequencies isn't satisfied.

3.5.1: FTIR Spectrometer Components

The three fundamental components of the FTIR system are the radiation source, Michelson interferometer, and detector. The Michelson interferometer is made up of a beam splitter, a fixed mirror, and a moving mirror. The Michelson interferometer is crucial because it divides IR rays in accordance with the sequence of their distinctive wavelengths. The two mirrors continue to be parallel with one another. These two mirrors have one that is stationary and the other that is free to move perpendicular to it. A further element of the FTIR setup is the beam splitter. It is made by depositing a thin layer of germanium (Gr) on a KBr substrate and is intended to be a semi-reflector. It has the capacity to divide the source light into multiple pieces, some of which reflect and some of which transmit. The radiations that hit the fixed mirror and were reflected proceed in that direction. The frequency ratios captured by prepared samples and kept in the interferograms are among the frequency-related details provided by interferograms **[8].** The interferogram converts the intensity (I) vs. frequency (f) IR spectrum using the Fourier transformation **[9].**

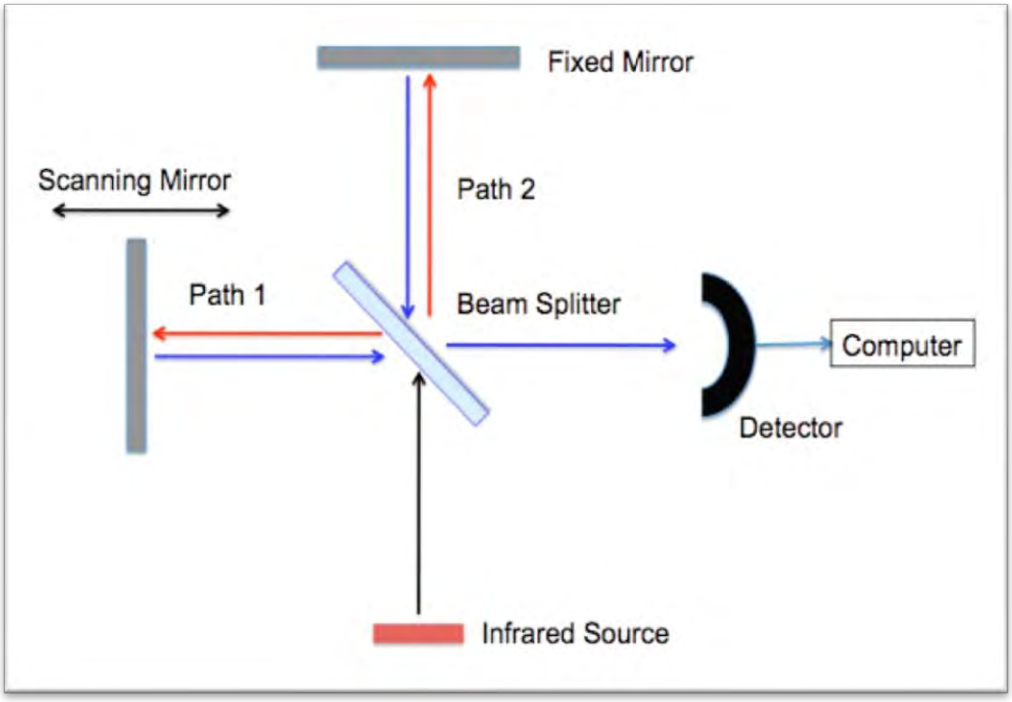

Figure 3.5 Illustration of Michelson interferometer

3.5.2: Procedure

The following techniques can be applied to the FTIR spectrum to examine the modes of vibration in ready superconducting samples:

- We utilised the OMNIC programme to extract data from the processed sample's produced spectrum.
- A prepared pallet of KBr is first placed in the beam's path (used as a background), and then 200 scans with a 400-700 cm^{-1} range are performed.
- Prior to preparing the pallet, we combined 50 mg of KBr that had already been thoroughly pulverised with 5 mg of the prepared sample. 200 more scans of the mixed sample spectrum were performed at the same range.
- We obtain the produced sample's spectrum after removing the KBr Spectrum's background.
- The spectrum of our samples was analysed and studied using OMNIC software tools.

FTIR can be used for the following purposes.

- Unknown materials identification
- Determination of a material's quality
- Measuring the amount of various components in a material

3.6 FLUCTUATION INDUCED CONDUCTIVITY (FIC) ANALYSIS

A technique for analysing superconducting fluctuations created by the production and annihilation of Cooper pairs down to the onset temperature is known as "fluctuation induced conductivity analysis" or "paraconductivity analysis." Cooper pairs begin to form above the transition temperature, but thermal turbulence causes them to keep forming and annihilating until T_c (R=0). Superconductor fluctuates as a result of production and annihilation. The density of fluctuation reduced when we cooled our sample below T_c (R=0), proving that thermodynamic fluctuation was ineffective in stopping the formation of a cooper pair. Since the cooper couples condensed as a result, there was no resistance **[10].**

These fluctuations in induced conductivity are observed for a temperature regime about T_c , which is referred to as the Ginzburg criterion temperature (T_G). For low temperature superconductors, T_G is less than 1 K, whereas for high temperature superconductors, it is between 1-2 K. Therefore, these variations could be looked at. As shown by the relationship below, Ginzburg was the first scientist to investigate how heat capacity fluctuations function and to develop the temperature value at which fluctuation adjustment to heat capacity is crucial.

$$\frac{\Delta T}{T_c} \sim \left[\frac{(T_c)^4}{\varepsilon_f}\right] \sim \left[\frac{(a)^4}{\xi}\right] \sim 10^{-4}\ to\ 10^{-16}$$

Here 'ξ' is coherence length and 'a' is the inter-atomic separation between two lattice sites. At higher temperatures, fluctuations that cause conductivity exhibit a deviation from its linear dependence, and it is represented as;

$$\Delta\sigma(T) = \frac{\rho_N(T) - \rho(T)}{\rho_N(T)\rho(T}$$

Where ρ (T) is the actual resistivity and $\rho_N(T) = \alpha + \beta T$ is the normal state resistivity.

Conductivity (T) is taken into account for two different kinds of fluctuations. One is Aslamazov-Larkin (AL) contribution, which describes excess current brought on by changes in the Cooper pair at temperatures above T_c **[11]**. The second article, Maki-Thompson (MT), talks about how superconducting carrier fluctuations affect how normal electrons conduct. The Lawrence-Doniach (LD) model is another model that sheds light on the boundary between two-dimensional (2D) and three-dimensional (3D) electronic states **[12].** As a result, FIC provides important information regarding the dimensionality, phase relaxation time, and coherence length of the superconductor, $\xi_c(T)$. The application of the LD model to assess crossover temperatures has received support from numerous studies, however due to the MT contribution's limited ability to evaluate, few researchers were persuaded. Although the results are slightly different from thin films, FIC analysis of polycrystalline bulk material is generally compatible with the feature of 3D fluctuation. 3D to 2D crossover has been observed in thin films with significant c-axis orientation. Temperature range affects how well 3D fluctuations or 2D-3D crossover perform. Different experimental outcomes have been found for a single crystal **[13].**

3.7 REFERENCES

[1] J. S. Blakemore, Solid State Physics, Cambridge University Press, (1985)

[2] Ashcroft, N.W. and N.D. Mermin, *Solid state physics (saunders college, philadelphia, 1976).* Appendix N, 2010. **166**.

[3] Ali, M.O., *Elementary Solid State Physics: Principles and Applications*. 1993: Addison-Wesley publishing company.

[4] Kittel, C., P. McEuen, and P. McEuen, *Introduction to solid state physics*. Vol. 8. 1996: Wiley New York.

[5] Alexander, L. and H.P. Klug, *Determination of crystallite size with the X-Ray spectrometer.* Journal of Applied Physics, 1950. **21**(2): p. 137-142.

[6] A Simplified Approach to the Solid State Physics, M.N Rudden, A.Inst. P.J. Wilson,

(1971)

[7] K. Lark-Horouitz and Vivian A.Johnson,Academic Press, New York and London

(1959)401-402

[8] J. R. Ferraro and L. J. Basile, Academic Press, 4(1982)345-392.

[9] F. A. Settle, Handbook of instrumental techniques for analytical chemistry. (Prentice Hall

[10] Larkin, A. and A. Varlamov, *Fluctuation phenomena in superconductors*, in *Superconductivity*. 2008, Springer. p. 369-458. PTR, (1997).

[11] L.G.A. and A.L. Larkin, Phy.Lett. A 26 (1968) 238–339.

[12] M. Muzaffar, M. Usman, N. A. Khan, Int J Mod Phys B 30.18 (2016) 1650112.

[13] S.J. Hagen, Z.Z. Wang, N.P. Ong, Phys. Rev. B 37.13 (1988) 7928

Chapter 4

RESULTS AND CONCLUSION

Different concentrations of Zinc were synthesized in CuTl-1223 sample by two steps solid-state reaction (SSR) technique at 860°C. The primary goal of this study is to explore the role of spin carrying entity in the mechanism of high T_c superconductivity. The planar reflection of all these samples corresponds to the orthorhombic crystal structure. The c-axes length slightly increases but the volume of the unit cell suppresses with increased Zn-doping in the final compound. $Cu_{0.5}Tl_{0.5}Ba_2Ca_2Cu_{3-x}Zn_xO_{10-\delta}$ (x=0, 1, 2, 3) samples indicate metallic variance of resistivity from room temperature through to the onset of superconductivity. Superconductivity onset temperatures were observed around in $Cu_{0.5}Tl_{0.5}Ba_2Ca_2Cu_{3-x}Zn_xO_{10-\delta}$ (x=0, 1, 2, 3) samples at 102.3, 104.3, 106.8, 108.1K and the zero resistivity critical temperature at 99.8, 90.4, 85.4, 86.5K, respectively. $TlBa_2Ca_2Zn_3O_{10-y}$ exhibits semiconductor-like resistivity variations with temperature ranging from 77K to 300K. The Mott 3D Varying Range Hopping (VRH) model was used for the experimental data of this sample. The energy of activation for $TlBa_2Ca_2Zn_3O_{10-y}$ was found around 2.9 meV. The phonon modes associated with the vibrations of apical and planar oxygen atoms are attenuated by Zn doping in the final compound. Excess conductivity (FIC) analyses of resistivity (ρ) vs. temperature (T) data have shown a suppression in the values of parameters like $\xi_{c(0)}$, J, and V_F with increased doping of Zn in the final compound. Since $\xi_{c(0)}$ depends on Fermi vector which in turn depends on density of carriers via $K_F = [3\pi^2 N/V]^{1/2}$ and it demonstrated density of carriers is suppressed with Zn doping. The values of $B_{c(0)}, B_{c1(0)}$ increases but the London penetration depth $\lambda_{p.d}$ decreases in all doped samples. The phase relaxation time of the carriers increases while the energy required to break the Cooper-pair decreases in all doped samples.

4.1 INTRODUCTION

In a unit cell of oxide superconductors the two most important constituents are (1) a charge reservoir layer (2) conducting $nCuO_2$ planes, where n=3 in current case. $Cu_{0.5}Tl_{0.5}Ba_2O_{4-\delta}$ charge reservoir due to its high position of the Fermi level supplies carriers to the

conducting planes. An intrinsic route cause of superconductivity in such compounds is yet unknown and a detailed experimental study in this direction are direly needed to unearth such hidden mystery **[1-8].** A basic question arises, "are only the free carriers responsible for superconductivity in CuO_2 planes of oxide superconductors or do other actors also play their part in this intriguing phenomenon?" The following are the significant players: (1) mass of atoms or phonons (2) Spins on the $Cu3d^9$ atoms (3) interactions between charge density and the spin of $Cu3d^{10}$ atoms. The spin of $Cu3d^9$ atoms in the background of oscillating nucleus initiates spin fluctuations and hence the charge density waves. In order to understand the underlying process of high T_c superconductivity in oxides superconductors we have opted for $Cu_{0.5}Tl_{0.5}Ba_2Ca_2Cu_3O_{10-\delta}$ samples due to their simple reproducible synthesis method and chemistry. In such compounds the superconductivity lies in their conducting CuO_2 planes and deficiency of carriers is covered by $Cu_{0.5}Tl_{0.5}Ba_2O_{4-\delta}$ charge reservoir. Flow of the carriers from charge reservoir layer towards the conducting CuO_2 planes is controlled by the higher Fermi level former. The $Cu3d^9$ atoms in the CuO_2 planes state carry a small spin. The spin on $Cu3d^9$ electrons begins to oscillate because of quantum mechanical oscillation of vibrating nucleus carrying charge. Such spin oscillations on individual $Cu3d^9$ sites interact with neighboring spins of copper sites consequently resulting into the spin density wave. There has not been much research done on the role of spin and hence the spin density wave in the mechanism of high temperature superconductivity yet. The main issue is whether the spin density wave plays a part in the development of phase coherence among the carriers in different CuO_2 planes and how it relates to the process of high T_c superconductivity. Therefore, to investigate the existence of such phenomena, we have Zn-doped samples with a concentration of x= 0, 1, 2, 3 in CuTl-1223; Zn being in the $3d^{10}$ state carry no spin. The increased concentration of Zn-doping would suppress the density of spins and if completely replaced with Zn in $Cu_{0.5}Tl_{0.5}Ba_2Ca_2Zn_3O_{10-\delta}$ samples the superconductivity should vanish provided there is no role of spin carrying entity in the mechanism causing high T_c superconductivity. To rule out any role of spin carrying entity in mechanism of high Tc superconductivity we have completely replaced the $Cu_{0.5}Tl_{0.5}Ba_2O_{4-\delta}$ charge reservoir layer by $TlBa_2O_{4-\delta}$ by synthesizing $TlBa_2Ca_2Zn_3O_{10-\delta}$ samples.

4.2 RESULTS AND DISCUSSION

4.2.1 Analysis of X-ray Diffraction

X-ray diffraction scans (XRD) of $Cu_{0.5}Tl_{0.5}Ba_2Ca_2Cu_{3-x}Zn_xO_{10-\delta}$ (x=0, 1, 2, 3) samples are shown in Fig.1.

Figure 4.1 The X-ray diffraction spectra of $Cu_{0.5}Tl_{0.5}Ba_2Ca_2Cu_{3-x}Zn_xO_{10-\delta}$ (x=0, 1, 2, 3) samples.

The planar reflection of all these samples corresponds to the orthorhombic crystal structure under PMMM space group, Fig 4.1. The c-axes length slightly increases whereas volume of the unit cell enhances with Zn-doping in the final compound, Table 4.1.

Sr#	Sample	a-axis	b-axis	c-axis	Volume
1.	$Cu_{0.5}Tl_{0.5}Ba_2Ca_2Cu_3O_{10-\delta}$	3.965	4.094	14.010	227.42
2.	$Cu_{0.5}Tl_{0.5}Ba_2Ca_2Cu_2ZnO_{10-\delta}$	3.776	3.964	14.024	209.91
3.	$Cu_{0.5}Tl_{0.5}Ba_2Ca_2Cu_1Zn_2O_{10-\delta}$	3.968	3.763	14.038	209.60
4.	$Cu_{0.5}Tl_{0.5}Ba_2Ca_2Zn_3O_{10-\delta}$	3.751	3.855	14.15	206.20
5.	$Tl_1Ba_2Ca_2Zn_3O_{10-\delta}$	3.778	3.845	14.002	203.40

Table 4.1: The a, b, c axes and volume parameters calculated from the XRD analysis of $Cu_{0.5}Tl_{0.5}Ba_2Ca_2Cu_{3-x}Zn_xO_{10-\delta}$ (x=0, 1, 2, 3) and $Tl\,Ba_2\,Ca_2\,Zn_3\,O_{10-\delta}$

Orthorhombic distortion climbs with increased Zn doping in the final excluding the sample with x=3. The changed orthorhombic distortion increased c-axes length. The decrease in the unit cell volume demonstrated the intrinsic doping of Zn in the final compound.

4.2.2 Temperature dependent resistivity measurements

Fig 4.2 displays the measurements of resistivity versus temperature of $Cu_{0.5}Tl_{0.5}Ba_2Ca_2Cu_{3-x}Zn_xO_{10-\delta}$ (x= 0, 1, 2, 3) samples.

Fig. 4.2 Temperature dependence of resistivity curves of $Cu_{0.5}Tl_{0.5}Ba_2Ca_2Cu_{3-x}Zn_xO_{10-\delta}$ (x=0, 1, 2, 3) samples.

As compared to the un-doped samples, the room temperature resistivity in Zn-doped samples increases. All $Cu_{0.5}Tl_{0.5}Ba_2Ca_2Cu_{3-x}Zn_xO_{10-\delta}$ (x=0, 1, 2, 3) metallic variance of resistivity has been seen in samples from room temperature to the onset of superconductivity. $Cu_{0.5}Tl_{0.5}Ba_2Ca_2Cu_{3-x}Zn_xO_{10-\delta}$ (x=0, 1, 2, 3) samples have shown onset of superconductivity around 102.3, 104.3, 106.8, 108.1K and the zero resistivity critical temperature at 99.8, 90.4, 85.4, 86.5K, respectively.

Sr.	Sample	Tc (R=0)	Tc (onset)

		K	K
1.	$Cu_{0.5}Tl_{0.5}Ba_2Ca_2Cu_3O_{10-\delta}$	99.8	102.3
2.	$Cu_{0.5}Tl_{0.5}Ba_2Ca_2Cu_2ZnO_{10-\delta}$	90.4	104.3
3.	$Cu_{0.5}Tl_{0.5}Ba_2Ca_2Cu_1Zn_2O_{10-\delta}$	85.4	106.8
4.	$Cu_{0.5}Tl_{0.5}Ba_2Ca_2Zn_3O_{10-\delta}$	86.5	108.1

Table 4.2: T_c and T_c onset of $Cu_{0.5}Tl_{0.5}Ba_2Ca_2Cu_{3-x}Zn_xO_{10-\delta}$ (x= 0, 1, 2, 3) samples

Samples without Cu in the final compound, i.e. $Tl_1Ba_2Ca_2Zn_3O_{10-y}$, have shown variable range hopping (VRH) conductivity that followed the relationship of the form:

$$\rho(T) = \rho_o \exp\left[\left(\frac{T_o}{T}\right)^{1/4}\right]$$

Employing Mott 3D VRH type conduction mechanism (with b = $\frac{1}{4}$) the $\rho - T$ data of numerous samples was analysed **[13].** The Mott 3D VRH model continues to a better fit for the experimental data of $TlBa_2Ca_2Zn_3O_{10-y}$ samples. It has semiconductor-like resistivity variations at temperature fitted in the range of (77-300) K as displayed in Figure 4.3.

Figure 4.3: Temperature-dependent resistivity measurement of Tl Ba_2 Ca_2 Zn_3 $O_{10-\delta}$ sample

In Fig 4.4 the inset represents the plot of ln ρ vs. $1/T^{1/4}$ and the theoretical prediction for the Mott Varying Range Hopping (VRH) in 3D mechanism is represented by a straight line that has given the energy of activation around 2.9 meV.

Figure 4.4: Activation energy curve of Tl Ba_2 Ca_2 Zn_3 $O_{10-\delta}$ sample

4.2.3 Fourier Transform Infrared Spectroscopy (FTIR) Measurements

Three FTIR absorption peaks belonging to the vibrations of two apical oxygen atoms of type $Tl - O_A - Cu(2)$, $Cu(1) - O_A - Cu(2)$ and a CuO_2 planar oxygen atoms can be seen in the spectra of $Cu_{0.5}Tl_{0.5}Ba_2Ca_2Cu_{3-x}Zn_xO_{10-\delta}$ (x=0, 1, 2, 3) samples. Three strong absorption modes relating to the vibrations are observed around 420-480 and 480-520 and 550-570 cm^{-1}, Fig.5.5

Figure 4.5: The FTIR absorption spectra of Zn doped CuTl-1223 with concentration (x=0, 1, 2, 3) samples superconductors

The peak position of the absorption band relating to the vibrations of $Tl - O_A - Cu(2)$ atoms remains almost unchanged and stays at 466cm^{-1} whereas the apical oxygen mode of type $Cu(1) - O_A - Cu(2)$ is softened with the increased doping of Zn in $Cu_{0.5}Tl_{0.5}Ba_2Ca_2Cu_{3-x}Zn_xO_{10-\delta}$ (x= 0, 1, 2, 3) samples. The CuO_2 planar oxygen mode is hardened with the doping of Zn in $Cu_{0.5}Tl_{0.5}Ba_2Ca_2Cu_{3-x}Zn_xO_{10-\delta}$ (x=0, 1, 2, 3) samples. The hardening of CuO_2/ZnO_2 planar oxygen mode in Zn-doped samples naturally arises due to larger mass of Zinc (65.39amu) in comparison with Copper (63.546amu) and increase in the c-axes length of unit cell. The effects of Zn-doped atoms on the intrinsic superconducting properties of $Cu_{0.5}Tl_{0.5}Ba_2Ca_2Cu_{3-x}Zn_xO_{10-\delta}$ (x=0, 1, 2, 3) samples have been evaluated by doing excess conductivity analyses of the conductivity data.

4.2.4 Excess Conductivity Analyses of $Cu_{0.5}Tl_{0.5}Ba_2Ca_2Cu_{3-x}Zn_xO_{10-\delta}$ (x=0, 1, 2, 3) Samples.

By applying fluctuation conductivity analyses (FIC) on conductivity data, the parameters determining intrinsic superconductivity in such samples are identified. These analyses were conducted using the "Aslamazov-Larkin(AL)" and "Lawrence-Doniach(LD)" models as represented by the results in Fig. 4.6(a, b, c, d).

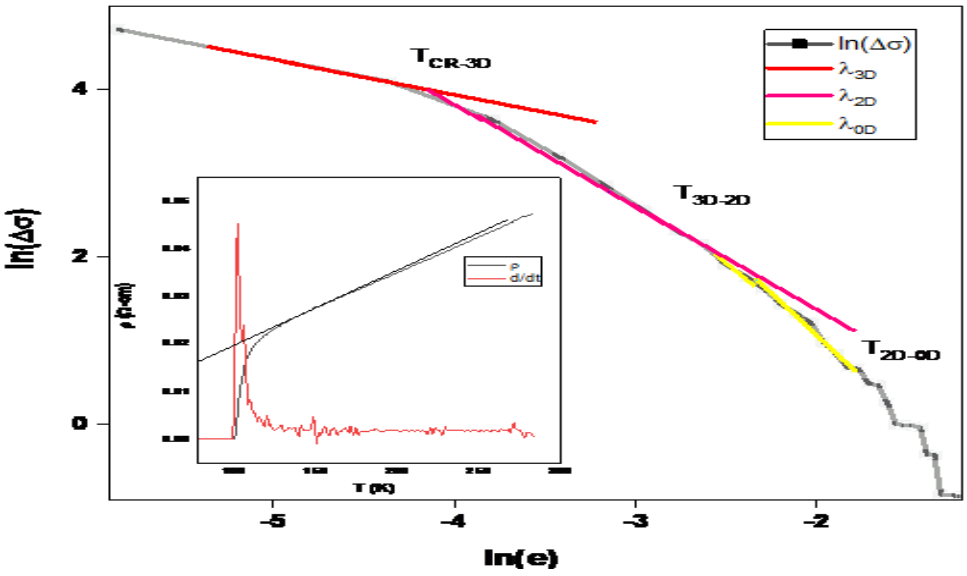

(a) x=0

(b) x=1

(c) x=2

(d) x=3

Figure 4.6 (a, b, c, d): Shows the illustrative figures of the excess conductivity analysis of superconducting $Cu_{0.5}Tl_{0.5}Ba_2Ca_2Cu_{3-x}Zn_xO_{10-\delta}$ (x=0, 1, 2, 3) samples.

The following equation is used for the excess conductivity analyses of $Cu_{0.5}Tl_{0.5}Ba_2Ca_2Cu_{3-x}Zn_xO_{10-\delta}$ (x=0, 1, 2, 3) samples:

$$\Delta\sigma_{(T)} = \Delta\sigma_{RT}\varepsilon^{-\lambda}$$

The form of this equation reads:

$$\ln \Delta\sigma_{(T)} = \ln \Delta\sigma_{RT} - \lambda_D \ln \varepsilon \qquad (1)$$

Where,

$$\varepsilon = \left[\frac{T - T_c^{mf}}{T_c^{mf}} \right]$$

It is called the reduced temperature and λ_D is the dimensional exponent; this equation is applicable to temperature around T_c and its surroundings. λ_D has values 0.3, 0.5, 1.0 and 2.0 related to critical, three-dimensional (3D), two-dimensional (2D) and zero-dimensional

(0D) respectively which are associated with various thermally activated processes **[9]**. For polycrystalline samples above expression can be modified as follows:

$$\boldsymbol{\Delta\sigma_{LD} = \left[\frac{e^2}{16\hbar d}\right](1 + Je^{-1})^{-1/2}\varepsilon^{-1}} \qquad (2)$$

The modification was proposed by Lawrence and Doniach (LD) and is known as LD model expression.

The $J = [2\xi_{c(0)}/d]^2$ in the above expression is inter-CuO_2-layers couplings, d is the thickness of superconducting layers (~15Å in present case) and the $\xi_{c(0)}$ is the coherence length along the c-axis.

From LD model the coherence length is computed based on the crossover temperatures by using this given expression **[10]:**

$$\boldsymbol{\xi_{c(0)} = \frac{d}{2}\left[\left(\frac{T_{3D-2D}}{T_{mf}}\right) - 1\right]^{1/2}} \qquad (3)$$

The phase relaxation time of the Cooper-pair can be derived using the equation below.

$$\boldsymbol{\tau_{\phi} = \frac{\pi\hbar}{8k_B T\varepsilon_o}} \qquad (4)$$

By using the phase relaxation time τ_{ϕ}, the coupling constant J:

$$\boldsymbol{J = (\hbar\tau_{\phi}^{-1})/(2\pi k_B)} \qquad (5)$$

The Fermi velocity of the carriers and the energy required to break apart the Cooper pairs is determined by using the equations that follow:

$$\boldsymbol{V_F = \left[5\pi k_B T_c \xi_{c(0)}\right]/2K\hbar} \qquad (6)$$

$$E = \frac{h}{[\tau_{\phi}(1.6\times10^{-19})]}eV \qquad (7)$$

the value of the proportionality co-efficient K≅0.12 is used as in reference **[11].**

Various crossover temperatures that result from different thermally activated process are T_G, $T_{3D\text{-}2D}$, $T_{2D\text{-}0D}$ determined via the log plot of the excess conductivity versus the reduced temperature Fig 4.6 and Table 4.3.

Sample	λ_{CR}	λ_{3D}	λ_{2D}	λ_{0D}	$T_{CR\text{-}3D}=T_G$ **(K)**	$T_{3D\text{-}2D}$ **(K)**	$T_{2D\text{-}0D}$ **(K)**	T_c^{mf} **(K)**	T^* **(K)**	$\alpha=\rho_n(0K)$ **(Ω-cm)**
x=0	-	0.50	1.30	2.20	103.35	114	123.37	98.00	128.17	0.015
x=1	-	0.47	1.40	2.02	102.35	110.38	120.38	96.71	120.19	0.024
x=2	-	0.52	1.42	1.82	97.34	103.36	104.37	92.50	115.66	0.026
x=3	-	0.54	1.14	2.01	102.35	104.35	105.36	99.18	122.26	0.20

Table 4.3: Superconducting-parameters from the plot of lnΔ(T) and ln ε of $Cu_{0.5}Tl_{0.5}Ba_2Ca_2Cu_{3-x}Zn_xO_{10-\delta}$ ***(x=0, 1, 2, 3) samples respectively.***

The intersection of several dimensional exponents yields these cross over temperatures i.e.

λ_{cr} = the slope below T_G,

λ_{3D} = the slope above T_G,

λ_{2D} = the slope above $T_{3D\text{-}2D}$

And

λ_{0D} = the slope of exponent value 2.

The parameters such as $\xi_{c(0)}$, the inter-layer coupling J, V_F (the Fermi velocity) of superconducting carriers and τ_φ (phase relaxation time of the carriers) are summarized for $Cu_{0.5}Tl_{0.5}Ba_2Ca_2Cu_{3-x}Zn_xO_{10-\delta}$ (x=0, 1, 2, 3) samples in Table 4.4.

Sample	**$\xi_c(0)$ (Å)**	**J**	**N_G**	**$\lambda_{p.d}$ x 10^2 (Å)**	**$B_{c(0)}$ (T)**	**B_{c1} (T)**	**B_{c2} (T)**	**K**	**$J_{c(0)}x10^3$ (A/cm^2)**	**V_F x10^7 (m/s)**	**E_{Break} (eV)**	**τ_φ x 10^{-13} (s)**
x=0	2.02	0.16	0.05	8.22	1.77	0.09	128.7	51.4	1.170	1.72	0.040	1.03
x=1	1.87	0.14	0.05	7.88	1.84	0.10	128.7	49.3	1.273	1.45	0.036	1.16
x=2	1.71	0.11	0.05	6.86	2.11	0.13	128.7	42.9	1.677	1.25	0.032	1.30
x=3	1.35	0.07	0.05	4.83	3.00	0.23	128.7	23.9	3.381	1.00	0.031	1.31

Table 4.4 Shows the superconductivity parameters observed from the FIC analysis of $Cu_{0.5}Tl_{0.5}Ba_2Ca_2Cu_{3-x}Zn_xO_{10-\delta}$ (x=0, 1, 2, 3) samples using the AL model.

The values of $\xi_{c(0)}$, J, and V_F suppress with the increased doping of Zn in the final compound. Such intrinsic superconductivity parameters depend on the density of superconducting carriers in the conducting CuO_2/ZnO_2 planes via Fermi-vector $K_F = [3\pi^2 N/V]^{1/2}$. A decrease in the values of these parameters with increased doping of Zinc suggested that their density is suppressed with doping of Zinc in the final compound. In such experiments it is vivid that the population spin carrying Cu $3d^9$ atoms suppresses that in result suppresses the density of spin density waves; the spin carrying electron is in the background of vibrating nucleus that oscillate and hence induce oscillations in the spin that results in the spin density waves. It was expected that decreased population of spin scattering atoms (i.e. Cu-atoms) would have increased the coherence length but it did other way round. On the other hand if the CuO_2 planes are completely replaced by ZnO_2 planes, the samples turn semiconducting. These observations suggest that there is an important role

of both spin carrying atoms and the density of carriers in the formation of superconductivity in such oxides. These findings have also revealed that the role of charge density is pivotal and role of spin density in the conducting planes is secondary.

The Ginzburg number N_G is yielded from the crossover temperature between 3D LD regime and the Ginzburg Landau (GL) regime. The crossover temperature is known as T_G. By using the T_G and T_c of a material, the equation for N_G reads:

$$\boldsymbol{N_G = \frac{T_G - {T_c}^{mf}}{{T_c}^{mf}}} \qquad (8)$$

Using N_G and the Ginzburg-Landau theory, key superconducting parameters are calculated **[12].** $\gamma = \frac{\xi_{ab(0)}}{\xi_{c(0)}}$ is the superconductor anisotropy which equals $\gamma = \frac{\xi_{ab(0)}}{\xi_{c(0)}} = \frac{5}{n-1}$ for CuTl-1223 samples with n=3 and leads to $\gamma = 2.5$ and the Ginzburg Landau (GL) parameter $\kappa = \lambda/\xi$**.** Here the point of inflection of the temperature derivative of resistivity $d\rho/_{dT}$ is used to determine the mean field critical temperature ($T_c{}^{mf}$).

Also $$N_G = \frac{1}{2}\left[\frac{K_B T_c}{{B_{c(0)}}^2 \gamma^2 {\xi_{c(0)}}^3}\right]^2 \qquad (9a)$$

And

$$\boldsymbol{B_{c(0)} = (K_B T_c / (2N_G)^{1/2} \gamma^2 \xi_{c(0)}^3)^{1/2}} \qquad (9b)$$

$$\boldsymbol{B_c = \frac{\Phi_0}{2\sqrt{2}\pi \lambda_{p.d(0)} \xi_{ab(0)}}} \qquad (10)$$

$$\mathbf{B_{c1} = \frac{B_c}{\kappa\sqrt{2}} \ln \kappa} \qquad (11)$$

$$\mathbf{B_{c2}} = \sqrt{2}\kappa \mathrm{B_c} \qquad (12)$$

$$\mathbf{J_c = \frac{4\kappa B_{c1}}{3\sqrt{3}\lambda_{p.d(0)} \ln \kappa}} \qquad (13)$$

Using Ginzberg Landau number N_G the parameters' values of $B_{c(0)}$, $B_{c1(0)}$, $B_{c2(0)}$, $J_c(0)$ and $\kappa = \lambda/\xi$ are determined by employing aforementioned equations (10) to (13) for Zn doped CuTl-1223 samples with concentration of (x= 0, 1, 2, 3). The values of the

parameters, $B_{c0}(T)$, $B_{c1}(T)$, $J_c(0)$, increase in all Zn-doped samples owing to enhanced flux pinning characteristics in $Cu_{0.5}Tl_{0.5}Ba_2Ca_2Cu_{3-x}Zn_xO_{10-\delta}$ (x=0, 1, 2, 3) samples. The lower density of superconducting carriers and smaller coherence length helps enhancing flux pinning characteristics that in turn results in suppressing $\lambda_{p.d}$ i.e. the London penetration depth, and the Ginzburg Landau (GL) parameter κ, see table 4.4. The energy required to break apart the Cooper-pairs into normal electrons in all Zn doped samples also decreases demonstrating weakly coupled superconducting electrons in Cooper-pairs of final compound, Table 4.4. Appearance of superconductivity in such $Cu_{0.5}Tl_{0.5}Ba_2Ca_2Zn_3O_{10-\delta}$ and its absence in $TlBa_2Ca_2Zn_3O_{10-\delta}$ samples demonstrated that existence of spin carrying Cu $3d^9$ is the key for the mechanism of superconductivity in such compounds. Since these spin carrying Cu $3d^9$ electrons are embedding an atomic nucleus having positive charge density that oscillate about its mean position which produce phonons. As result of oscillations of nucleus the Cu $3d^9$ electrons spin in turn oscillates too that in turn produces spin density waves. These observations have shown that spin density wave is essential for the mechanism of high T_c superconductivity.

4.3 CONCLUSIONS

Superconducting properties of $Cu_{0.5}Tl_{0.5}Ba_2Ca_2Cu_{3-x}Zn_xO_{10-\delta}$ (x=0, 1, 2, 3) samples are studied by preparing the samples by two-step solid-state reaction (SSR) method. X-ray diffraction analysis of these $Cu_{0.5}Tl_{0.5}Ba_2Ca_2Cu_{3-x}Zn_xO_{10-\delta}$ (x=0, 1, 2, 3) samples have shown that these samples grow in orthorhombic crystal structure in which their c-axes length increases and the volume of the unit cell suppresses with increased Zn-doping. Metallic variation of ρ versus T(K) is typical feature of $Cu_{0.5}Tl_{0.5}Ba_2Ca_2Cu_{3-x}Zn_xO_{10-\delta}$ (x=0, 1, 2, 3) samples; $TlBa_2Ca_2Zn_3O_{10-\delta}$ sample has, however, shown semiconducting behavior. $Cu_{0.5}Tl_{0.5}Ba_2Ca_2Cu_{3-x}Zn_xO_{10-\delta}$ (x=0, 1, 2, 3) samples have shown onset of superconductivity around 102.3, 104.3, 106.8, 108.1K and the zero resistivity T_c at 99.8, 90.4, 85.4, 86.5K, respectively. $TlBa_2Ca_2Zn_3O_{10-y}$ sample has shown semiconductor-like resistivity variations that followed Mott Varying Range Hopping (VRH) in 3D with temperature. The activation energy of thermally activated processes in such samples fitted the regime of 77K to 300K has given an energy of activation around 2.9 meV. The phonon modes associated with the vibrations of apical and planar oxygen atoms are attenuated by

doping of Zn in the final compound. The ρ vs. temperature data of excess conductivity (FIC) analyses has shown a decrease in the values of parameters like $\xi_{c(0)}$, J, and V_F with increased doping of Zn in $Cu_{0.5}Tl_{0.5}Ba_2Ca_2Cu_{3-x}Zn_xO_{10-\delta}$ (x= 0, 1, 2, 3) samples. These parameters are highly dependent on density of carriers via $K_F = [3\pi^2 N/V]^{1/2}$ and the suppression in the values of these parameters suggested that doped Zn-atoms promote a drop in the density of carriers. The values of $B_{c(0)}$, $B_{c1(0)}$ increase with Zn-doping showing that density of inadvertent defects increases with the doping of Zn acting as pinning; the London penetration depth $\lambda_{p.d}$ decreases in all doped samples. The phase relaxation time, τ_φ, of the carriers increases but the energy required to break- apart the Cooper-pair decreases in all doped samples. These studies have unequivocally demonstrated the importance of spin carrying $Cu3d^9$ atoms in the mechanism of high T_C superconductivity; doped Zn atoms suppress it and hence the superconductivity.

4.4 REFERENCES:

[1] Xiao, G., Cieplak, M.Z., Gavrin, A., Streitz, F.H., Bakhshai, A., Chien, C.L.: Phys. Rev. Lett., 60(1988) 1446.

[2] A. Raza, S. H. Safeer, N. A. Khan : J. Superconductor and Nov. Mag., (2016)

[3] Kandyel, E., Sekkina, M.A., Dawoud, M.A.T., Bohnam, M.Y.: Solid State Commun. 135 (2005) 214–219.

[4] Tominoto, K., Terasaki, I., Rykov, A.I., Mimura, T., Tajima, S.: Phys. Rev. B, 60(1999) 114.

[5] Hidekazu Mukuda, Sunao Shimizu, Akira Iyo, and Yoshio Kitaoka: J. Phys. Soc. Jpn. 81 (2012).

[6] Fukuzumi,Y.,etal.:Phys.Rev.Lett.76 (1996) 684.

[7] C. W. Chu, L. Z. Deng and B. Lv.: Physica C, 514(2015)290-313.

[8] . Hudson, E.W., Lang, K.M., Madhavan, V., Pan, S.H., Eisak, H., Uchida, S., Davis, J.C.: Nature, 411(2001)920

[9] L. G. Aslamasov and A. I. Larkin, "The influence of fluctuation pairing of electrons on the conductivity of normal metal," *Physics Letters A*, vol. 26, no. 6, pp. 238–239, Feb. 1968, doi: 10.1016/0375-9601(68)90623-3.

[10] A. K. Ghosh, S. K. Bandyopadhyay, P. Barat, P. Sen, and A. N. Basu, "Fluctuation-induced conductivity of polycrystalline Y1−xCaxBa2Cu3O7−δ superconductors," *Physica C: Superconductivity*, vol. 264, no. 3–4, pp. 255–260, Jun. 1996, doi: 10.1016/0921-4534(96)00257-2.

[11] A. L. Solovjov, H.-U. Habermeier, and T. Haage, "Fluctuation conductivity in YBa2Cu3O7−y films with different oxygen content. II. YBCO films with Tc≈80 K," *Low Temperature Physics*, vol. 28, no. 2, pp. 99–108, Feb. 2002, doi: 10.1063/1.1461921.

[12] Sarmiento, M.R., et al., "*Conductivity fluctuation and superconducting parameters of the YBa2Cu3− x (PO4) xO7–δ material,"* Physica B: Condensed Matter, vol.398, no.2s, pp. 360-363,2007.

[13] L. Essaleh, S. M. Wasim, G. Marín, C. Rincón, S. Amhil, and J. Galibert, "Mott type variable range hopping conduction and magnetoresistance in p-type CuIn3Te5 semiconductor compound," *Journal of Applied Physics*, vol. 122, no. 1, p. 015702, Jul. 2017, doi: 10.1063/1.4991004.